Long-span roofs:
Design solutions for **free-edge barrel vault gridshells**

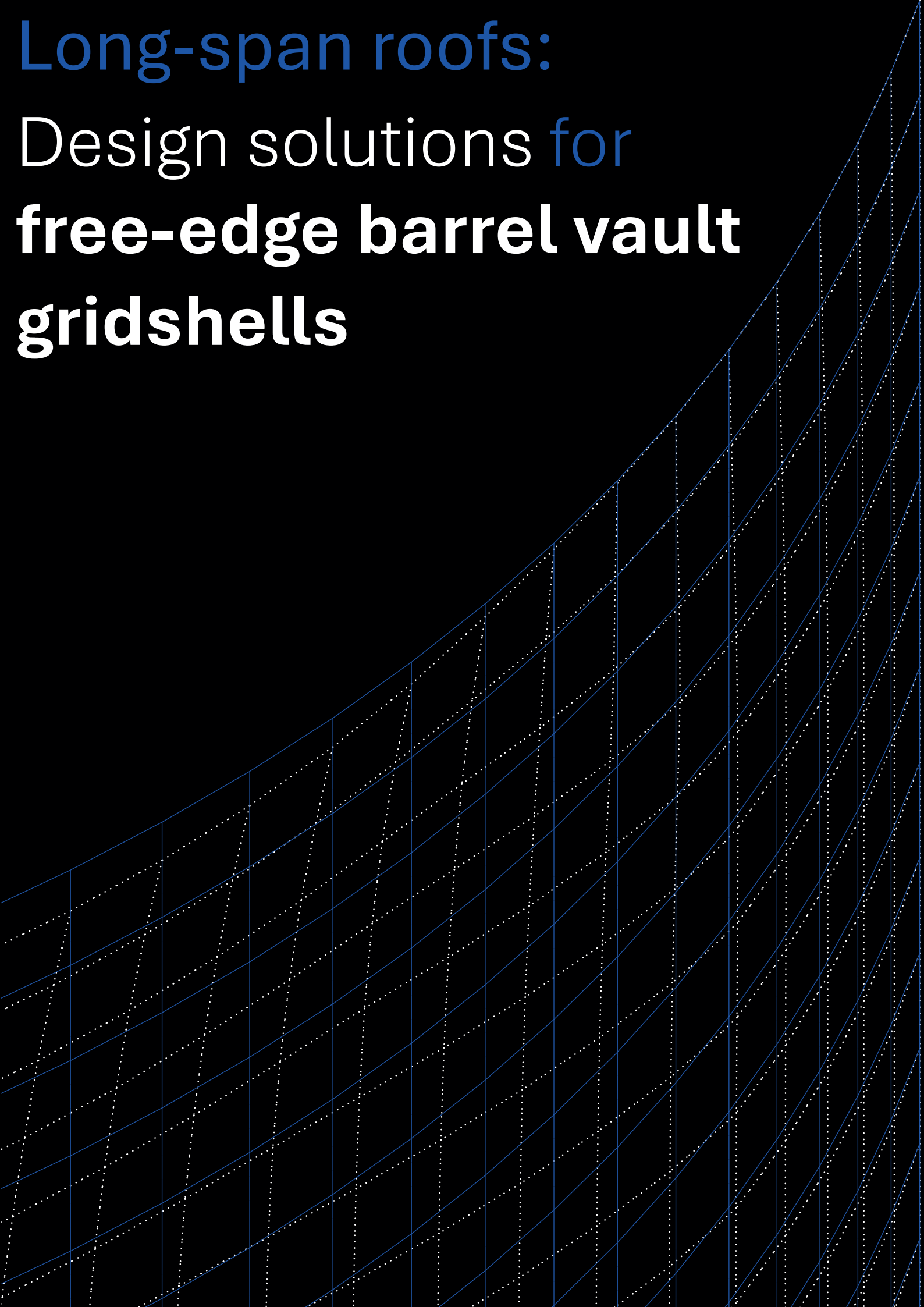

POLITECNICO DI TORINO

Master Degree in Architettura Costruzione Città

MSc Thesis

December, 2024

Long-span roofs:
Design solutions for free-edge barrel vault gridshells

Politecnico di Torino

DAD
Dipartimento di Architettura e Design

Supervisors:
Luca Bruno
Fiammetta Venuti
Lorenzo Raffaele

Candidate:
Sara Bordigoni Pistorello

Constantly researching for equilibrium

To Mien,
always on the same side

In costante ricerca di equilibrio

A Mien,
sempre dalla stessa parte

Acknowledgements

Before switching language, I wish to express my sincere gratitude to all the people from around the world who have helped broaden my horizons throughout this journey.
A heartfelt thanks to all my colleagues at the *École Polytechnique fédérale de Lausanne*, especially to Daniel for the boundless enthusiasm and Kenyan vibes.

Prima ancora di raccontare questo lavoro di Tesi, mi è doveroso volgere i miei ringraziamenti a tutti coloro senza i quali le prossime pagine sarebbero completamente bianche.

Ai miei Relatori tutti, per avermi dedicato il loro prezioso tempo, con costante presenza e solerte attenzione, per la fiducia riposta in me nel prendere parte al lavoro di ricerca e soprattutto per aver reso possibile che questo periodo di studio e redazione della Tesi di Laurea sia stato da me trascorso come il più sereno di tutto il periodo universitario.
Galeotta fu una lezione del primo anno sulla concezione strutturale della *Maison à Bordeaux* di Rem Koolhaas!

Alla società di ingegneria Sintecna, in particolare al Prof. Paolo Napoli per avermi permesso di svolgere il tirocinio curricolare attorno alla tematica delle strutture di grande luce, in linea con il tema generale della Tesi di Laurea Magistrale.

Alla mia famiglia per aver reso possibile questo percorso, lasciando alla mia testa dura la facoltà di gestirlo autonomamente, fidandosi a lasciar vivere in solitaria la mia insolita personalità.
A mamma Laura, che ogni volta è riuscita a caricarmi il peso di un bilico di cibo sulle spalle, nonostante tornassi a casa con lo zaino più piccolo che possedessi. Alla fine però, il vero motivo di quel peso era l'amore che, tra un *bulacco* di pesto e un *toco di fügassa*, ritrovavo sempre quando tornavo a Torino e disfacevo lo stesso zaino vuoto con cui tornavo a casa.
A papà Luca, per aver sempre desiderato stappare *"una bella bottiglia"* ad ogni mio rientro a casa (e avermi messo ogni volta in stato di ebbrezza), per aver lasciato la mia -già al tempo- anima solitaria giocare con i mattoncini *Lego*, ora so che in realtà avrebbe anche lui voluto partecipare alle mie costruzioni.

Ringraziamenti

A fratellone Diego, iniziatore della fuga dal mare verso la grande città, ingegnere, razionale e disciplinato, *Kosmos* della famiglia, nonché il mio esatto opposto.
A tutti i miei nonni, per ogni *"quando torni a casa?"* chiesto.
Al nonno, che al lavoro gli architetti li mandava in un certo posto, volato via troppo presto per poterci mandare anche me.

A Elena per la sua anima buona,
A Jo per la sua esplosione di colori,
A Flavio per il suo essere sempre sorridente,
A Simone per la sua pronta risposta ad un milione di dubbi digitali.

A tutti i personaggi incontrati lungo questo percorso che hanno condiviso con me le stesse vicende.
A Giulia, compagna di avventure Svizzere, unica persona che ha condiviso con me l'emozione di dormire letteralmente sul pavimento di una serra, contornate da piante di pomodori e abbracciate dal freddo della campagna Belga e che, nonostante ciò, ha percorso di pari passo a me la strada che ci ha condotte verso questa meta, condividendo intere giornate di lavoro, consigli e idee.

Ai miei cari Prof. Egildo e Prof. Church, per non essere mai stati intimoriti da quella ragazzina che leggeva Nietzsche all'angolo della scuola, ma averne preso una mano per metterla sul foglio a disegnare linee e curve e l'altra a pigiare tasti di una chitarra.

A Mien, figura cardine lungo tutta la mia *stairway to heaven*, l'unico che di questi anni ha vissuto luci e ombre, nutrendo sempre profonda stima in me e sopportando ogni mio disequilibrio con una infinita pazienza, la stessa che ci ha messo leggendo questa Tesi man mano che veniva scritta. Ha accettato la mia distanza quando avrebbe preferito avermi vicina, colta nel pensiero e raccolta da ogni paranoia. Prima persona a cui ho sempre condiviso idee, scelte e strategie, e unica persona che ho trovato sempre dalla mia stessa parte.

Abstract

For millennia, long-span roofs have held significant importance in both architectural and engineering fields, evolving alongside technological advancements in materials and their intrinsic properties.

The concept of gridshell emerged within this framework as a lightweight, form-resistant structural typology capable of spanning large distances with minimal material thickness and weight. This revolutionary aspect enabled gridshells to be widespread worldwide, especially where lightness and transparency were paramount design criteria. The membrane-like structural behaviour of gridshells involves the high degree of structural efficiency of these structures, but also results in a propensity for buckling instability, which have been studied over time.

The need to adapt gridshells to existing structures as well as ensuring accessibility has led gridshells to be designed with free-edges. They are achieved by trimming the reference surface and result in breaking the continuity of their spring line. The free-edges significantly compromise the membrane behaviour of gridshells, and potentially involve bending internal forces and large displacements, in addition to persisting stability issues.

The present MSc Thesis aims to propose design solutions for free-edge gridshells and to assess their structural performances. The study takes advantages of the recent FreeGrid benchmark intended to fill the gap between design practice and scientific research. Specifically, the current study focuses on the Barrel vault Design Baseline Geometry (DBG), proposed by the benchmark as one of the references, with the aim of testing Design Solution Gridshells (DSGs) that enhance the performance of the DBG and restore the membrane behaviour. The assessments were conducted through a holistic approach, synthesized by FreeGrid into partial metrics of Structural performance, Buildability performance and Sustainability performance.

The initial phase of the research focused on the Ultimate Limit State (ULS) and Seviceability Limit State (SLS) analyses of the DBG mechanical behaviour through a 3D Finite Element Model. Based upon these latter analyses, several DSGs were proposed, conceived from both traditional and uncommon strategies for free-edge gridshells. For each DSG, a preliminary ULS and SLS analysis returned as output two main Structural performance partial metrics: the critical Load Factor from the load-displacement curve, identifying the instability regime at ULS; the maximum vertical displacements at SLS. These evaluations served as a touchstone for assessments of the Structural performances among the DSGs and with reference to the DBG.

With these premises, the second phase was devoted to the detailed analysis of few DSGs, selected as the most effective in terms of Structural performance. For each of these DSGs, the ULS assessment provided as outputs the load-displacement curve linked to element plasticization; the SLS assessment evaluated maximum normal and tangential displacements, axial forces and bending moments, all normalized with respect to the corresponding peak values of the DBG. Lastly, for each selected DSG, partial performance metrics as well as the overall performance metric were computed and evaluated in relation to the DBG.

The analyses revealed that each DSG successfully reinstates the dominance of membrane behaviour over the flexural one, thereby reducing the occurrence of fully and partially plasticized members and shifting each gridshell into a global instability regime rather than the local one. The selected DSGs marked an improvement in Structural performance terms with respect to the DBG, although none satisfied the displacement threshold established by the benchmark. Additionally, each DSG exhibited an enhancement in the overall Bulk metric, despite the decrease in Buildability and Sustainability performances.

In light of these assessments, the future phasis of research could involve final sizing of structural members as well as testing further shape variations, with the aim of fulfilling the threshold set by the benchmark.

List of Figures

List of Tables

Contents

Chapter

1

Introduction

For millennia, long-span roofs have represented a focal point for the technological and architectural interest, first serving as expression of power and mark of identity. Later on, they evolved to guarantee the fulfillment of functional requirements, evolving over the time in terms of materials as a consequence of their intrinsic properties.

Due to the transition from the use of materials with a high dead load to live load ratio to those with a reduced one, it has been possible to drive forward the advancing of experimentations, leading to increase the complexity of structural configurations with reduced construction time and costs.

This development has marked a significant advancement in the field of Structural Engineering and therefore in Architecture, enabling the attainment of long-span roofs covered by elements with a minimal thickness. In ancient times, such achievement would have been unattainable as the use of bricks and lithoid materials -not effective in resisting tensile stress- required considerable thickness to ensure the stability of vaults, arches, or domes. The increase of thickness assured that the thrust line generated by the structural weight would remain within the section, even under the influence of the applied load (Majowiecki, 2012).

Throughout history, design efforts have been targeted to the reduction of the ratio between dead load and live load. The achievement of this latter goal was enabled by introducing materials with enhanced mechanical properties, thus achieving a decrease of over 100-fold. This research reached a turning point during the Second Industrial Revolution when steel production was greatly enhanced by the Bessemer converter, by which steel was established as a hallmark of the groundbreaking innovation of the period.

The effectiveness in reducing the dead-to-live load ratio was ensured by the fact that, combined with concrete, steel could be used to withstand tensile stress, allowing for more complex and wider geometries.

In this backdrop, pioneering figures of Eduardo Torroja (1899-1961) (Figure 1.1-a), Félix Candela (1910-1997) (Figure 1.1-b), Nicolas Esquillan (1902-1989) (Figure 1.1-c), Heinz Isler (1925-2009) (Figure 1.1-d) stood out for using the steel-concrete combination to design form resistant structure.

(a) Zarzuela Hippodrome, Eduardo Torroja (Madrid, 1935)

(b) Los Manantiales Restaurnat, Félix Candela (Mexico City, 1958)

(c) Norwich Sports Village Hotel, Heinz Isler (Norwich, 1991)

(d) CNIT, Nicolas Esquillan (Paris, 1958)

Figure 1.1: Examples of steel-concrete shells

Despite of these fascinating experimentations, the steel-concrete combination had a negative impact on the labor costs and the need for specific curve formwork. These factors explain the reason why the widespread adoption of these structures was hindered.

With this background, engineers and architects began to envision alternative solutions to overcome long-span spaces, recognizing the greater potential of steel to further minimize the amount of structural material.

In the late '50s of 20th Century, Frei Otto established the theoretical framework for the development of a new, lightweight structural type compared to the thin opaque shells previously tested, also introducing the possibility of transparency to allow light to pass through. He identified this innovative structure as *Gitterschale*, translated as Gridshell (Liddell, 2015).

Although the first known application of a double-curved grid structure dates back to the 1897, pioneered by engineer Vladimir Shukhov in the Vyksa Steel Production Hall (Figure 1.2), it was in the second half of the 20th Century that significant advancements were made in this field. The research was led by the work of Frei Otto, as well as by contributions of Buckminster Fuller, Jörg Schlaich e Hans Schober of Schlaich Bergermann und Partner, who collaborated to define technological and design principles for gridshell structures.

Frei Otto developed the concept of post-formed timber gridshell, exemplified by the Multihalle Pavilion for the Mannheim Bundesgartenschau in 1975 (Figure 1.3), building one of the greatest timber gridshells and among the lightest compression structures ever built; Richard Buckminster Fuller patented the geodesic dome typology (Figure 1.4), focusing on spherical surfaces, referring to gridshells domes (Carlini and Tedeschini Lalli, 2019); Jörg Schlaich and Hans Schober focused on steel and glass, bending-inactive or pre-formed gridshells (Bruno and Venuti, 2018) in the roof of the Swimming Bath Aquatoll in Neckarsulm (Figure 1.5), standing as one of the earliest examples in this sense.

Subsequent research has greatly broadened the application of the gridshell concept, driven by these emblematic examples, and enabled its widespread use across the world in a variety of materials and typological declensions.

Figure 1.2: Vyksa Steel Production Hall, Vladimir Shukhov (Vyksa,1897)

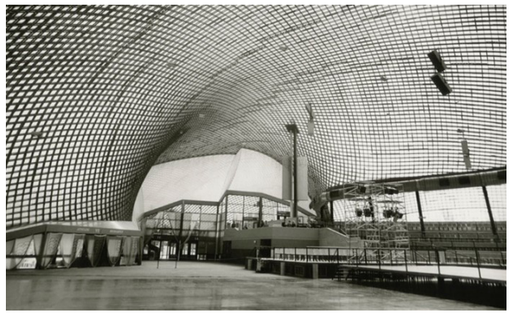

Figure 1.3: Multihalle Pavilion, Frei Otto (Mannheim, 1975)

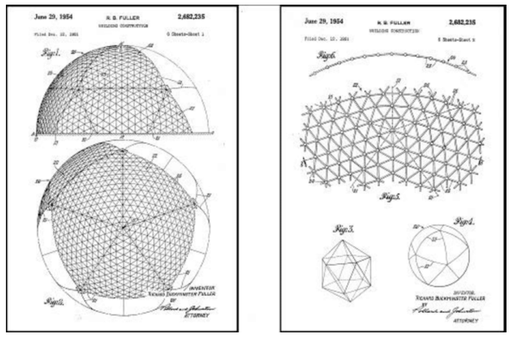

Figure 1.4: Patent for Building Construction, Richard Buckminster Fuller (1954) (Carlini and Tedeschini Lalli, 2019)

Figure 1.5: Swimming Bath Aquatoll, Schlaich Bergermann und Partner (Neckarsulm, 1990)

Whereas in the early 1960s geometries of gridshells were constrained to limited surface types, advances in computational technology, in particular nonlinear Finite Elements Analysis (FEM), have allowed design to explore far more complex geometries.

The efficiency and optimization of gridshell structures have to face the huge number of variables that affect their structural performance, often leading to instability phenomena. As a notable example, the collapse of the Bucharest Exhibition Hall dome in 1970 shifted research focus towards the mechanical behaviour of gridshells.

The elasto-plastic stability phenomena affecting these structures is still nowadays an open research topic, particularly regarding the stability of free-edge gridshells and the effects in elastic boundary structures (Bruno and Venuti, 2018). Despite this challenge, free-edge gridshells are widely used in practical design.

In light of these premises, the present work was undertaken subsequent to the FreeGrid international benchmark (https://sites.google.com/view/freegrid), launched at the IASS Annual Symposium 2023 in Melbourne. The aim to bridge the gap between practical design and scientific literature (Bruno *et al*, 2023-a), is led by FreeGrid by establishing a unified reference for the design and engineering of free-edge steel gridshells. To accomplish this latter goal, the benchmark proposes to compare and test various approaches on three baseline geometries: barrel vault, parabolic dome, hyperbolic paraboloid.

In alignment with the benchmark guidelines, this study focuses on the barrel vault with its predefined characteristics and aims to test various solutions to address the posed questions and to improve the metrics of Structural performance, Buildability and Sustainability, compared to the barrel vault baseline geometry.

More broadly, this work seeks to contribute to the scientific research on free-edge steel gridshells, highlighting potential future directions in the design of gridshells and, more generally, long-span roofs and the architectural implications that may arise.

Chapter

2

Gridshells in Architecture

Definition of Gridshell **2.1.0**

It is no coincidence that the conception of this structural typology by Frei Otto occurred at the Institut fur leichte Flächentragwerke of Stuttgart (or Institute of Lightweight Structures). When we refer to gridshells we are indeed identifying first of all a typology belonging to the category of lightweight structures with a high span-to-thickness ratio (Schlaich, 2011), able to cover large spans through the geometric configuration. Gridshells are form-resistant structures (Bruno and Venuti, 2018), meaning that they ideally carry loads through in-plane normal forces (membrane behaviour) rather than through bending moments (Bruno and Venuti, 2018; Van der Linden, 2015; Raffaele *et al*, 2024). For this reason, gridshells are able to achieve large spans with minimal thickness. As in shell structures, the presence of bending moments would lead to significant deformations because of the relatively low flexural stiffness compared to the axial one.

However, the main mechanical distinction between gridshells and shells lies in the absence of a continuous solid surface (Figure 2.1), so the load is restricted to flow along the grid elements, as opposed to shells where infinite load paths are available across the continuous surface (Van der Linden, 2015).

Because of their lightness and ability to span wide open spaces, gridshells are particularly suited for structures that demand transparency and lightness as well as spatial characteristics, such as wide spaces free from structural obstructions and internal flexibility. As such, they represent an efficient solution for designing sport facilities, like stadia and swimming pools, industrial buildings, as hangars and airport terminals, social buildings, as pavilions and auditoriums, for covering existing courtyards and even for temporary installations.

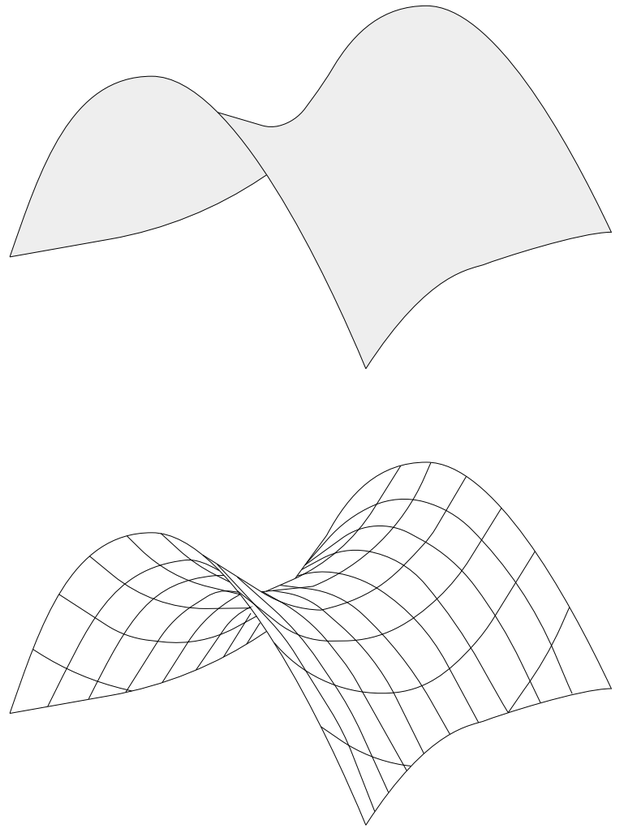

Figure 2.1: Shell and Gridshell

Morphology

The combination of these efficiency and adaptability factors has enabled the widespread adoption of gridshells worldwide, giving rise to distinctive structures and innovative shapes. Notably, it is the shape itself that assumes a key role when discussing the structural behaviour of gridshells.

Defined as a structure with the shape and strength of a double-curvature shell, but made of a grid instead of a solid surface (Douthe, 2006), it becomes clear that the geometrical configuration of a gridshell must be understood as a structural form (Dyvik and Mork, 2015), i.e. the geometry cannot be only determined by preconceived design choices but it must strike the balance between architectural aesthetics and mechanical performance of the structure.

Since Frei Otto's earliest experimentations in Essen (Songel, 2020), the pursuit of structural form involved the use of the Hooke's hanging chain method, traditionally adopted to model compressed structures since Giovanni Poleni (1683-1761) (Chilton, 2016) (Figure 2.2), Antoni Gaudí (1852-1926) (Perrson, 2023) (Figure 2.3), Heinz Isler (1926-2009) (Boller, 2024) (Figure 2.4), for instance.

He used the same principle in order to obtain an optimized geometry for compression through the inverted hanging chain, as the model for the Mannheim Multihalle shows (Figure 2.5).

The key distinction that defines gridshells as form-resistant structures is that their shape is exclusively dictated by the presence of forces. There are several important parameters to guide the conceptual form-finding of a form-resistant structure: if a portion of the surface tends to be flat, configuration can arise bending deformation phenomena due to the structural tendency to behave like a beam. On the other hand, if the surface is curved, the configuration benefits an advantageous distribution of forces. As demonstrated in Heinz Isler's test, a straight element bears less load than a curved one and for shells case, it allows the structure to withstand out-of-plane loads through in-plane forces (Persson, 2023). As a matter of fact, the optimal geometry is defined by a double-curved surface , which does not necessarily has to be symmetrical (Figure 2.6-a). An efficient geometry also occurs when the curvature is highly pronounced in one direction and flat in the other one (Figure 2.6-b). The structural efficiency can also be

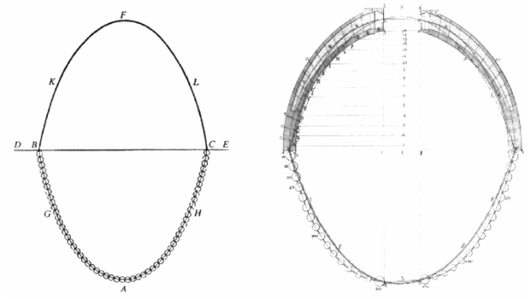

Figure 2.2: Hooke's analogy between arch and hanging chain and analysis of the Dome of St.-Peter's in Rome, Giovanni Poleni (1748)
(Block *et al*, 2006)

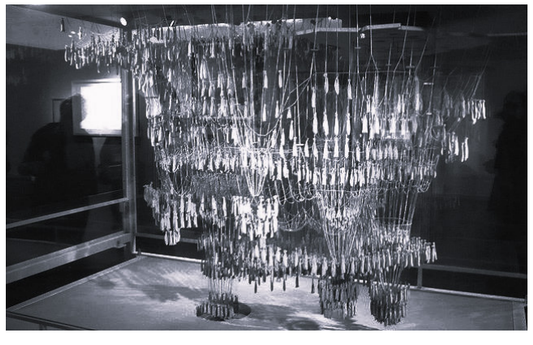

Figure 2.3: Sagrada Familia hanging chain model, Antoni Gaudí (1889)
(Fernandes *et al*, 2016)

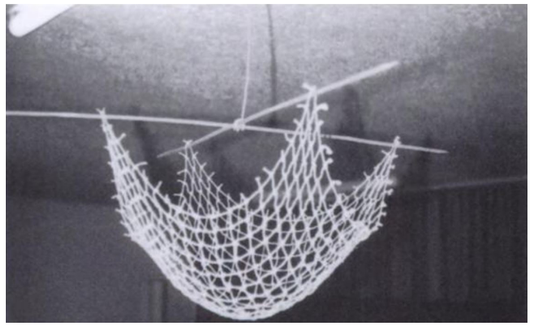

Figure 2.4: Hanging membrane model with unstiffened free edges, Heinz Isler
(Chilton, 200)

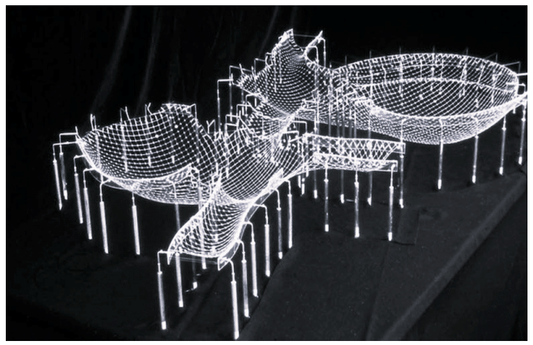

Figure 2.5: Mannheim Multihalle Pavilion model, Frei Otto
(Liddell, 2015)

compromised by the presence of folds or prominent cantilever edges (Dyvik and Mork, 2015) (Figure 2.6-c). In addition to this, the membrane behaviour can be modified when the geometry has holes or free-edges (Figure 2.6-d) which lead the shell to bending moments.

From a morphological standpoint, the geometric nature of the shape can be considered focusing on the fundamental geometric elements that define the spatial configuration of gridshells.

When the arch-shape generatrix, or a semi-circle in geometrical terms, is translated along a straight directrix, the result will be a single curvature configuration, known as barrel vault (Figure 2.7-a).

If this translation first occurs along a vertically oriented parabolic arch and then along a horizontally oriented one, the resulting geometry will be a hyperbolic paraboloid, or more precisely a ruled double-curved surface with positive curvature in one direction and negative in the other one (Rockwood, 2015) (Figure 2.7-b).

If the generatrix is revolved around a vertical straight axis instead of being translated, the configuration will be a dome, defined by a double-curved surface with entirely positive curvature (Figure 2.7-c).

Within double-curved surfaces, it is possible to distinguish between synclastic geometries, where loads are transferred either entirely through compression or tension (Figure 2.8-c), and anticlastic surfaces such as the hyperbolic paraboloid, which are more efficient in resisting out-of-plane instability although exhibiting both stresses in combination (Van der Linden, 2015) (Figure 2.8-b).

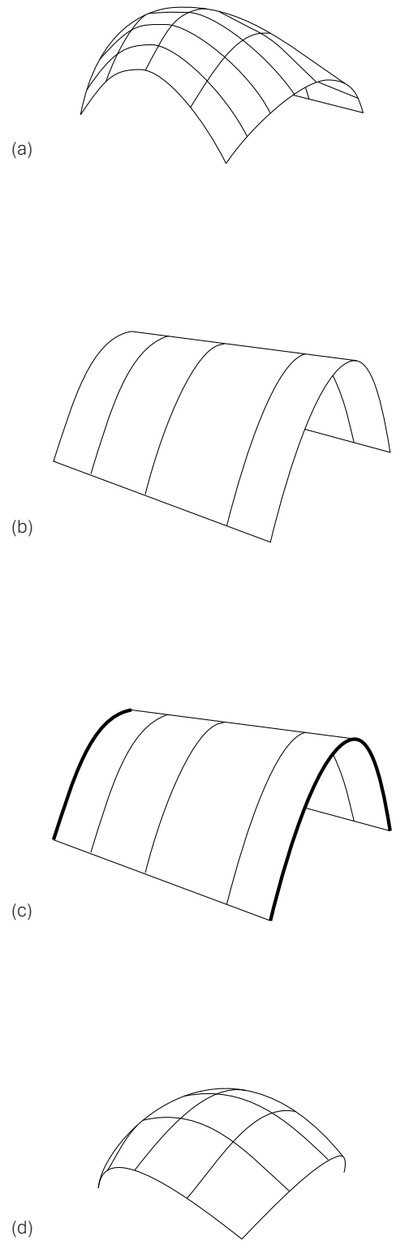

Figure 2.6: Form finding concept parameters

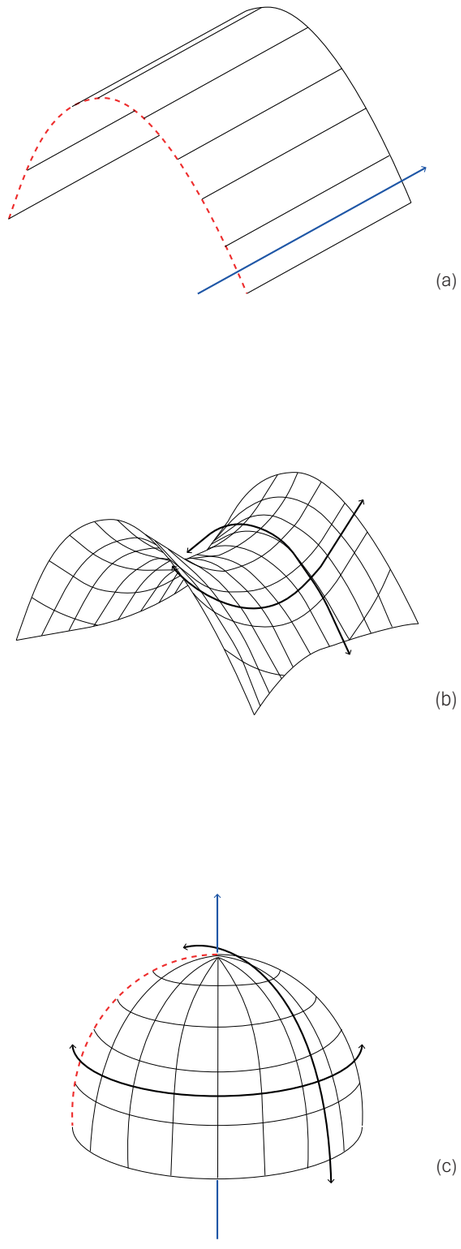

Figure 2.7: Reference and trimming surfaces of geometries: barrel vault (a), hyperbolic parabolic (b), dome (c)

Figure 2.8: Synclastic (b) and anticlastic (c) double-curved surfaces

Classification 2.3.0

In order to analyze the various factors involving in the design of gridshells, a range of evaluation methods can be outlined. The following classification is based on a comparative criterion which relates to construction methods, boundary conditions, geometric aspects and different materials.

Bending-active and post-formed Gridshells 2.3.1

The construction process approach of a gridshell establishes differences between structure conceived as bending-active or elastic, and post-formed.
Bending-active gridshells are linked to the concept of developable surfaces (Van der Linden, 2015), where the structure starts from a planar grid then deformed into its final shape, through a kinematic process, which requires shear stiffening by locking the nodes of the grid and adding bracings (Mesnil, 2013) (Figure 2.9).
Post-formed gridshells are generally classified as non-developable structures instead, meaning that they cannot be flattened without undergoing geometrical alterations. As a result, they are better suited to resist internal forces and provide greater rigidity compared to elastic gridshells (Faber, 1963). In this case, the grid elements are typically discretized into straight segments, whereas in bending-active gridshells they follow the curvature of the surface (Dyvik *et al*, 2021) (Figure 2.10).

Fully-constrained and free-edge Gridshells 2.3.2

Examining various examples of built gridshells, it becomes clear that the final shape is often achieved by trimming the geometry with horizontal, vertical, inclined planes or even curved surfaces, thus giving rise to elastic boundary structures.
About this issue, a recent research (Bruno and Venuti, 2018) classifies gridshells in two categories: a first type where the geometry is trimmed by a single surface, giving rise to springlines that rigidly constrain the structure (Figure 2.11-a); a second type where the geometry is intersected by multiple planes. In this case the spring lines result from one cut, while the other

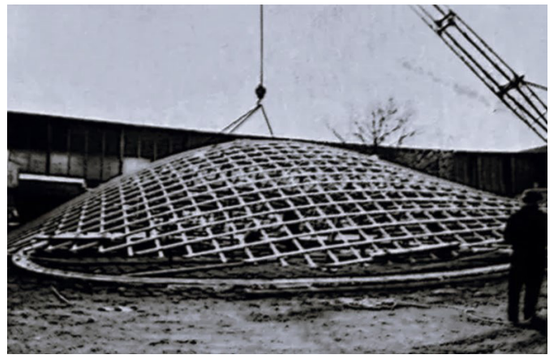

Figure 2.9: 9 Building process of Frei Otto's Essen bending-active gridshell
(Drew, 1976)

Figure 2.10: Building process of Frei Otto's Mannheim bending-inactive gridshell

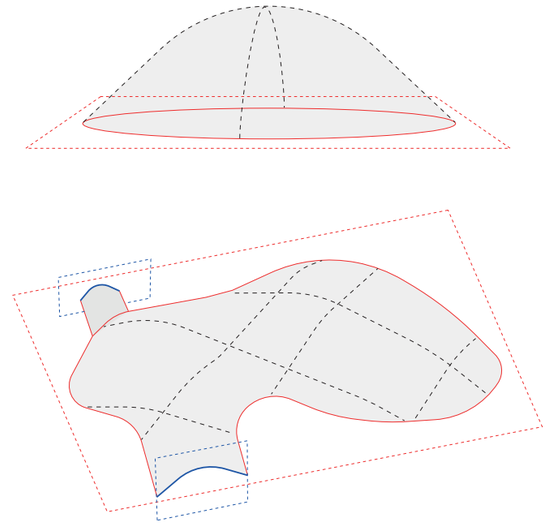

(a) Frei Otto's Essen gridshell

(b) Frei Otto's Mannheim gridshell

Figure 2.11: Example of fully-constrained (a) and free-edge (b) gridshell

give rise to free-edges (Figure 2.11-b). These are known as free-edge gridshells, where the structural design is further more challenging due to the fact that the membrane behaviour is compromised by the presence of unrestrained edges (Raffaele *et al*, 2024). The study of the structural behaviour of free-edge gridshells represents a gap in the scientific literature, even though free edges are commonly seen in constructed gridshells, often serving as access points to buildings or as integrations with existing structures, features hardly achievable using fully-constrained gridshells.
In realized examples of free-edge gridshells, stiffening the free edge and adding vertical elements to reduce its free length are the most widely adopted strategies to address the challenges due to the presence of elastic boundaries (Bruno and Venuti, 2018).

2.3.3 Single-layer and double-layers Gridshells

The geometry of gridshells can also be classified based on the number of layers they consist of, generally distinguishing single-layer and double-layer gridshells.
Single-layer gridshells consist of a grid lying on a single surface (Figure 2.12-a). While they are efficient at distributing stresses evenly, however they are susceptible to out-of-plane bending behaviour and to shell-like buckling (IASS WG8, 2014) due to the action of external loads on the structure (Figure 2.13-a). Several studies (Kato *et al*, 1998; Fan *et al*, 2011; Van der Linden, 2015; Grande *et al*, 2018; Zhang *et al*, 2022) have examined the joints effect and their stability to better understand this phenomenon.
Despite these challenges, single-layer gridshells offer advantages in terms of buildability semplicity, cost-efficiency and the ability to suit complex geometries.
Double-layers gridshells are an extension of this system, involving multiple planes - typically parallels - connected to each other (Figure 2.12-b). These structures are significantly more rigid against bending, thanks to the connection between upper, lower and diagonal elements, yet they are prone to member buckling before the entire structure reaches shell-like global buckling (IASS WG8, 2014) (Figure 2.13-b).

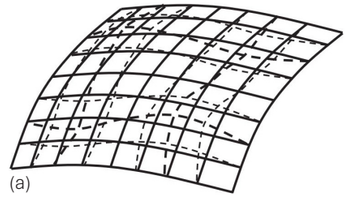
(a)

(a) British Museum Great Court, Foster and Partners (Camden, 2000)

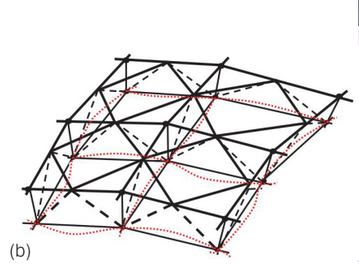
(b)

Figure 2.13: Single-layer (a) and double-layers (b) buckling (IASS WG8, 2014)

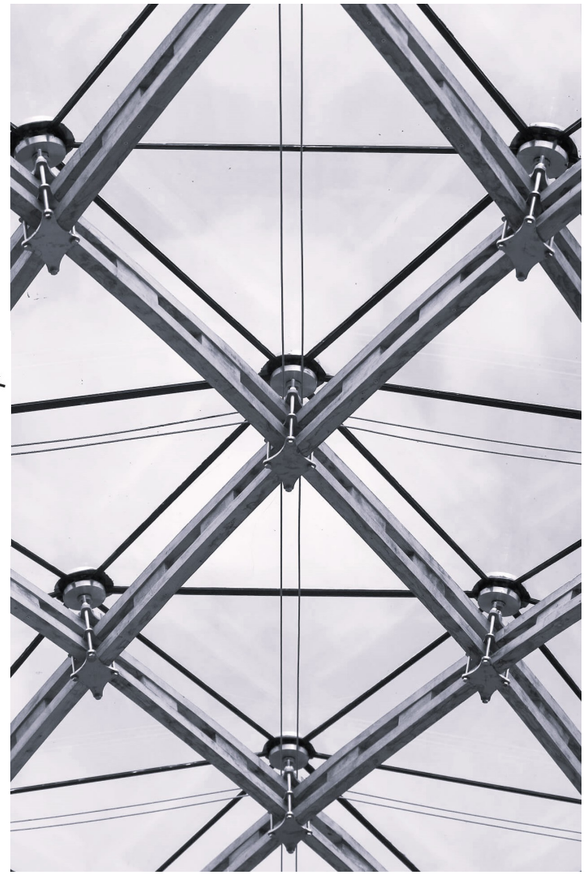
(b) Chiddingstone Orangery gridshell, Buro Happold (Chiddingstone, 2004)

Figure 2.12: Example of single-layer (a) and double-layers (b) gridshell

Mesh patterns

Regardless the number of layers composing the gridshell and the overall geometry, the grid is made up by the sum of smaller, repetitive units that together define the geometry, replacing the continuous surface of traditional shells. The typological regularity of these units holds aesthetic, constructive and, most importantly, structural values (Bruno *et al*, 2023-a). The most widespread are quad mesh and triangular mesh patterns.

Quad mesh patterns (Figure 2.14-a-1) are particularly suited for the design of elastic gridshells (Dyvik *et al*, 2021), especially in the kinematic process (Dyvik and Mork, 2015) as they can easily accept variations of angles during geometric deformation (Songel, 2020). However, they often require the addition of brace cables to triangulate the mesh, without which the necessary in-plane shear stiffness and membrane behaviour would not be ensured (Van der Linden, 2015; Boling, 2021). Conversely, triangular mesh patterns (Figure 2.14-b-2), as the name suggests, inherently provide in-plane stiffness and the corresponding structural advantages, though it is less effective in handling out – of - plane forces (Majowiecki, 2012). Other types of patterns have been recently introduced, such as hexagonal (Figure 2.14-c) and Voronoi-like topology (Tonelli *et al*, 2016) (Figure 2.14-d-3). In all cases, achieving planar faces is advantageous for economic reasons - curved panels would significantly increase costs - and for structural analysis, as planar elements reduce degrees of freedom in the structure (Persson, 2023). While triangular mesh patterns inherently ensure planarity of faces, other patterns require alternative methods to achieve this (Raffaele *et al*, 2024).

A second classification can be based on the orientation of the base units i.e. orthogonal or diagonal to the cutting planes. The distinction becomes clear when examining the grid elements: orthogonal mesh patterns (Figure 2.15-a) require the elements to follow more pronounced curvatures compared to diagonal mesh patterns (Figure 2.15-b), and this challenge increases with the rise of the gridshell (Dyvik and Mork, 2015).

Specifically, the free-edge and grid-layout orientations lead to different structural behaviour.

A gridshell is defined as anisotropic when the grid pattern is

(a) Schubert Club Band Shell,
Schlaich Bergermann und Partner
(St. Paul MN, 2002)

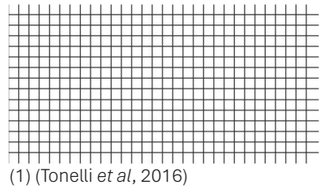

(1) (Tonelli *et al*, 2016)

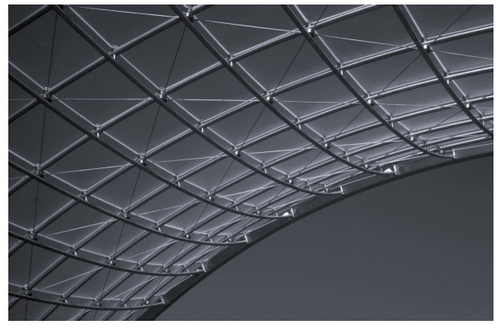

(b) Roof of the Madrid Palacio de Comunicaciones,
Schlaich Bergermann und Partner
(Madrid, 2009)

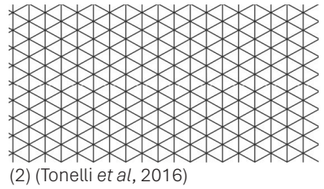

(2) (Tonelli *et al*, 2016)

(c-d) Mock-up of static-aware Voronoi free-form
grid shell vault,
Structural Laboratory of University of Pisa
(Froli and Laccone, 2017)

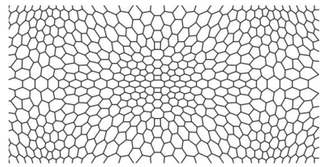

(3) (Tonelli *et al*, 2016)

Figure 2.14 Gridshell mesh patterns: quadrangular (a-1), triangular (b-2), hexagonal (c), Voronoi-like (d-3)

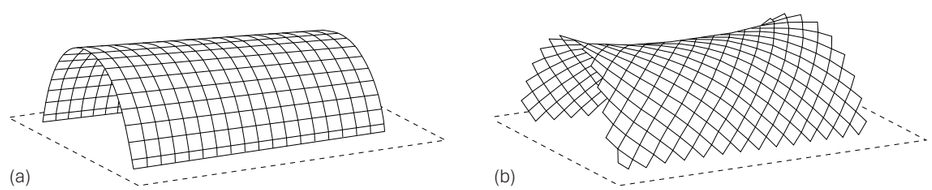

Figure 2.15: Gridshell mesh patterns: orthogonal (a), diagonal (b)

oriented differently from the cutting plane. Furthermore, some authors classify gridshells with equilateral cell mesh patterns as isotropic, differently from orthotropic ones. Notably, regarding instability resulting from variations in free-edge orientation, orthotropic gridshells are significantly affected, unlike isotropic gridshells (Venuti, 2021).

Materials

2.4.0

Among the gridshells constructed so far, a relatively recent study (Dyvik *et al*, 2021) shows that -for cases where the material is known- the majority are made of steel (Figure 2.16), wood (Figure 2.17) results widely employed, and fewer examples use bamboo (Figure 2.18) or composite materials (Figure 2.19). The choice of material is closely tied to the construction process: wood and bamboo, although both anisotropic materials and therefore not capable of defining true gridshells (Rockwood, 2015), are well suited to the kinematic construction method due to their high flexural performance (Dyvik and Mork, 2015; Rockwood, 2015; Van der Linden, 2015).

While wood was the first material used in early experimentations about gridshells, bamboo has been more recently explored as a sustainable option. However, its construction techniques are not yet completely defined in literature, particularly concerning its tendency to fracture during bending (Nurdiah *et al*, 2023) and the challenge of standardizing connections between bamboo elements because of the variable size of nodes (Rockwood, 2015).

On the other hand, steel gridshells are necessarily constructed using pre-formed elements (Raffaele *et al*, 2024), typically derived from the discretization of the continuous reference surface, assembled on site, thus not subjected to strain (Persson, 2023). The ability to span large distances with low percentage of structural material is ensured by the high strength of steel, which has contributed to the widespread use of steel gridshells, often combined with glass surfaces.

Although gridshells have been explored as an optimization of concrete shells, the idea of constructing grid structures from concrete has rarely been pursued (Persson, 2023), as even with the reduced use of material, special formworks would

Figure 2.16: Schluterhof Roof,
Schlaich Bergermann und Partner
(Berlin, 2002)

Figure 2.17: Weald and Downland gridshell,
Buro Happold
(Singleton, 2002)

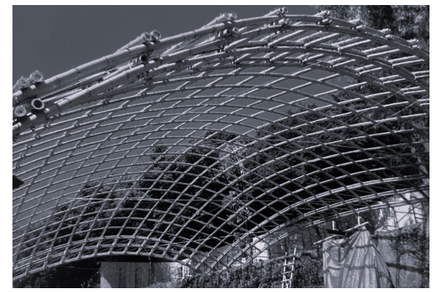

Figure 2.18: Bamboo gridshell at UNAM campus,
research team led by Juan Gerardo
Oliva Salinas
(Mexico City, 2011)
(Chilton, 2016)

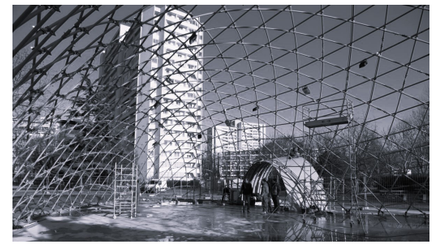

Figure 2.19: Ephemeral Cathedral,
T/E/S/S
(Créteil, 2013)

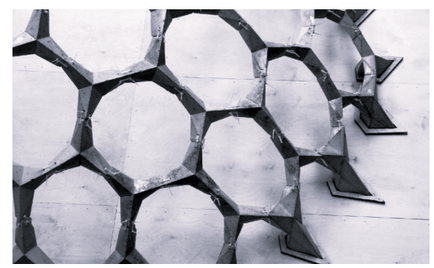

Figure 2.20: Concrete gridshell pavilion,
Aarhus School of Architecture
(Aarhus)
(Pedersen, 2013)

still be required. Notable research of the Aarhus School of Architecture sought to overcome this limitation by proposing a concrete gridshell composed of connected, triangularized units (Pedersen, 2015), tested for the design of a pavilion, but it remains a single experimental case (Figure 2.20).

Main issues in the design of Gridshells

2.5.0

As previously discussed, the development and widespread application of gridshells in architecture have been driven by their efficiency in spanning wide spaces with minimal thickness, enabling the creation of aesthetically fascinating and functional structures such as providing wide spaces free from structural members. Despite these advantages, several factors that complicate the apparent ease of designing gridshells must be considered.

A main aspect to be discussed concerns the structural behaviour of gridshells. The collapse due to instability has been over time a significant focus of the research about these structures and it still is nowadays considered by the scientific community the main cause of their structural failure (Gioncu, 1985).

In general, for single-layer gridshells, failure occurs at a stress level lower than the yield strength of the material. This happens because of small displacements from the undeformed configuration, which significantly reduce the stiffness of the structure (Majowiecki, 2012), ultimately leading to its collapse.

The typologies of collapse can be different depending on the specific class of gridshell and the nature of instability can be classified as follows:

-local instability, when the collapse affects one or more nodes;

-global instability, when the entire structure collapses, as seen in single-layer gridshells (IASS WG8, 2014);

-element instability, where the failure of an element does not immediately compromise the entire structure, as can happen in double-layers gridshells (IASS WG8, 2014);

-combined instability, which combines the previously mentioned categories (Bulenda and Knippers, 2001).

Several factors can influence the stability of gridshells, including Gaussian curvature (Abel and Chilton, 2011) which varies

according to the geometric nature of the structure; grid typology (Bruno and Venuti, 2018; Raffaele *et al*, 2024); joint rigidity (Kato *et al*, 1998; Fan *et al*, 2011; Van der Linden, 2015; Grande *et al*, 2018; Zhang *et al*, 2022); geometric imperfections (Bulenda and Knippers, 2001); boundary conditions, in particular concerning free-edge gridshells, for which a limited percentage of scientific studies exists (Bruno and Venuti, 2018; Gioncu, 1995). Regarding this latter variable, there is a notable lack of specific information in literature despite numerous free-edge gridshells examples in the design practice, which have been built using various solutions for elastic boundary structures.

A further consideration can be done regarding buildability of gridshells. Since gridshells geometries can exhibit varying degrees of complexity, from a construction point of view this leads to increased construction costs - a particularly significant factor for free-form, double-curved and post-formed gridshells where elements may have different length and non-standard joints (Raffaele *et al*, 2024).

This issue generally does not interest elastic gridshells where both joints and lengths of the elements can be unvaried throughout the grid. Nonetheless, an economic sustainability challenge for elastic gridshells lies in the potential lack of planar faces, i.e. when a gridshell is created using kinematic process by raising a flat grid with quad mesh pattern, the surfaces remain undiscretized and this means that the resulting cladding panels cannot be planar.

From a sustainability perspective, yet another consideration can dome. In the current context, designing the possibility to reduce the amount of structural material can be read as an opportunity to address sustainability issues. Beyond the quantitative aspect, attention has to be given to the qualities of materials, specifically the potential to build gridshells using non-conventional materials with efficient intrinsic properties and lower embodied energy (Raffaele *et al*, 2024).

Chapter

3

The FreeGrid Benchmark

This chapter refers to the technical specifications defined in FreeGrid documentation (Bruno *et al*, 2023-a, b, c, d, e, f, g, h; Raffaele *et al*, 2024).

Introduction: Aims and Goals 3.1.0

The state of the art presented has shed light on the wide range of aspects that define gridshells. It highlights that their design cannot be confined to a single thematic discipline, but it must reflect multidisciplinary expertise instead, engaging with various, possible approaches and addressing goals of different nature.
In response to this, the FreeGrid Benchmark has been promoted with the aim of providing a common reference point for testing and comparing different approaches to design and optimization methodologies within the field of gridshells.

Launched at the Annual Symposium of the International Association for Shell and Spatial Structures IASS2023 held in Melbourne in July 2023, FreeGrid addresses seven general problem statements, each aligned to specific goals related to the following themes:
-the polarization in gridshell engineering between the phasis of modeling/analysis and practice/application, which FreeGrid seeks to bridge;
-the multidisciplinary nature of gridshell design and optimization, which FreeGrid aims to bring together by gathering expertise from different fields;
-the wide range of approaches to the structural concept of form-resistant structures, ranging from heuristic, trial-and-error methods based on the designer's experience to optimization techniques and artificial intelligence;
-the occurrence of free-edges in gridshells, which compromise the assumption of perfectly rigid constraints, promoting FreeGrid to fill this gap in current scientific literature;
-the multiple goals that holistic design activities must satisfy, for which FreeGrid establishes performance metrics;
-the reproducibility of results, for which FreeGrid adopts an Open Data policy applied to the data and tools provided to and required from participants;
-the impartiality of evaluations, which FreeGrid ensures by

introducing performance metrics that guarantee objective and quantitative control.

For this purpose, FreeGrid adopts three geometrically, structurally defined reference case studies, called Design Baseline Gridshells, (DBGs) and establishes a methodological framework to be applied in their analysis. Each participant in the challenge is required to contribute by improving the overall performance of the three DBGs. To achieve this goal, each of them has to develop their own design solutions by modifying the baseline geometry according to constraints and criteria set by the benchmark.

Figure 3.1: FreeGrid logo

Design Baseline Gridshells: geometry 3.2.0

The three gridshells identified by FreeGrid as DBGs refer to geometries of barrel vault (Figure 3.2-a), parabolic dome (Figure 3.2.b) and hyperbolic paraboloid (Figure 3.2-c).
Belonging to the class of single-layer gridshells, the three case studies differ in the typology of curvature, single curvature (barrel vault), double Gaussian positive (parabolic dome) and double Gaussian negative (hyperbolic paraboloid).
The three geometries share the following common characteristics:
-the boundary condition, defined by the presence of a free-edge which partially releases the spring-lines;
-the equation governing the parabolic generatrix, expressed as follows:

$$z = -\frac{x^2}{2B} + f \quad , \quad \mathrm{D} = \left\{ -\frac{B}{2} \le x \le \frac{B}{2} \right\}$$

where the generatrix span is B=30m; the rise f=B/8; the horizontal reference plane z=0.
The generatrix arc length is defined as:

$$\mathrm{A} = \mathrm{B}\left[\frac{\sqrt{5}}{4} + ln\left(\frac{1+\sqrt{5}}{2}\right)\right] \approx 1.04B$$

It defines 20 edges with constant length $b = A/20 \approx 1.56$m along the edge of both generatrix and directrix.
The directrix equation has a domain defined by:

$$\left\{ -\frac{B}{2} \le y \le \frac{B}{2}, x=0 \right\}$$

which differs among the three-design baseline gridshells, and it is described in Table 1 for each DBGs, where H is the maximum length above the horizontal reference plane z; L is the length of the continuous spring line, L^* is the length of the free-edge, S is the surface area encircled by the projections of the free-edge, the continuous spring line and the end arches on the horizontal reference plane z;
-discrete translational surfaces with a homogeneous mesh described by planar square faces bxb, except for those along boundaries;
-the grid density, which is therefore $1/(b^2/2) \approx 0.82$ [$1/m^2$], with a tributary area of 1.217 m^2 for each structural member, excluding those at the edges.

	Barrel vault	Parabolic dome	Hyperbolic paraboloid
directrix generatrix	$z = f$ $\mathrm{B} = \left\{ -\frac{B}{2} \le y \le \frac{B}{2}, x=0 \right\}$	$z = -\frac{y^2}{2B} + f$ $\mathrm{B} = \left\{ -\frac{B}{2} \le y \le \frac{B}{2}, x=0 \right\}$	$z = \frac{y^2}{2B} + f$ $\mathrm{B} = \left\{ -\frac{B}{2} \le y \le \frac{B}{2}, x=0 \right\}$
H	$B/8$	$B/8$	$B/4$
L	A	$\frac{2\pi B}{3}$	$\frac{3}{2B}$
L^*	L	$L/2$	L
S	BL	$\pi B^2/4$	$\pi B^2/2$

Table 1: DBGs geometrical specifications

3.3.0 Design Baseline Gridshells: structural conditions

3.3.1 Structural members

The three reference gridshells are defined by steel members with bilinear elastic-perfect plastic constitutive law with material properties summarized in Table 2.
Each structural member has a hollow circular cross-section not subjected to precompression. The geometric characteristics outlined in Table 3, are common among members of each case study, yet they differ across different Design Baseline Gridshells.

steel grade	density	Young's modulus	Poisson's ratio	yield strength
355	ρ = 7850 kg/m³	E = 2.1e + 5 MPa	ν = 0.3	f_y = 355 MPa

Table 2: Material properties

	Barrel vault	Parabolic dome	Hyperbolic paraboloid
Section type (type, diameter, thickness)	O/139.7/14.2	O/101.6/10	O/101.6/10
Area [mm^2]	5596	2876	2876
Inertia [mm^4]	11157936	3052611	3052611

Table 3: DBGs cross-sections main properties

Structural constraints 3.3.2

Both internal and external boundary conditions are defined for the three gridshells in Table 4.
Internally, the structures have perfectly rigid joints which prevent rotational movements between converging members.
Externally, the structural joints along the edge L are constrained by perfect hinges, except for the barrel vault where the arches are constrained against translations only along the *x* and *z* axis, while displacements in the y direction is permitted to prevent non-lineare stiffening effect induced by elements along the same direction. The joints are not constrained along the free-edge *L**.

	Barrel vault	**Parabolic dome**	**Hyperbolic paraboloid**
internal joints	Rigid (δ_x , δ_y , δ_z , r_x , r_y , r_z)		
external joints along L	Pinned (δ_x , δ_y , δ_z)		
external joints along head arches	δ_x , δ_z	-	-
external joints along L*	Free		

Table 4: DBGs boundary constraints

Load conditions 3.3.3

The evaluation of baseline geometries and design solutions must take into account two load conditions LC_i, with i=1:2. (Figure 3.3)
These conditions are ideally and simplistically determined with the intent to evaluate performance under ideal, controlled load settings, with magnitudes that are comparable to the standard design loads typically used for gridshells.
The first load condition LC_1 refers to a symmetric, distributed load which is the sum of the members self-weight and point loads applied in each joint $Q_{1,k}= (q_1+q_2)s_k$, where s_k is the projected area of influence of the *k*-th joint on the reference plane *z*=0 and q_1,q_2 represents respectively the uniformly distributed load of the glass cladding weight and snow load.
The second condition LC_2 refers to an asymmetric load intended to simulate non-uniform vertical loads and horizontal loads induced by wind or other horizontal forces. It includes the members self-weight and the point loads $Q_{2,1,k}=q_1 s_k$ applied to the surface with $x > 0$ for the barrel vault and parabolic dome

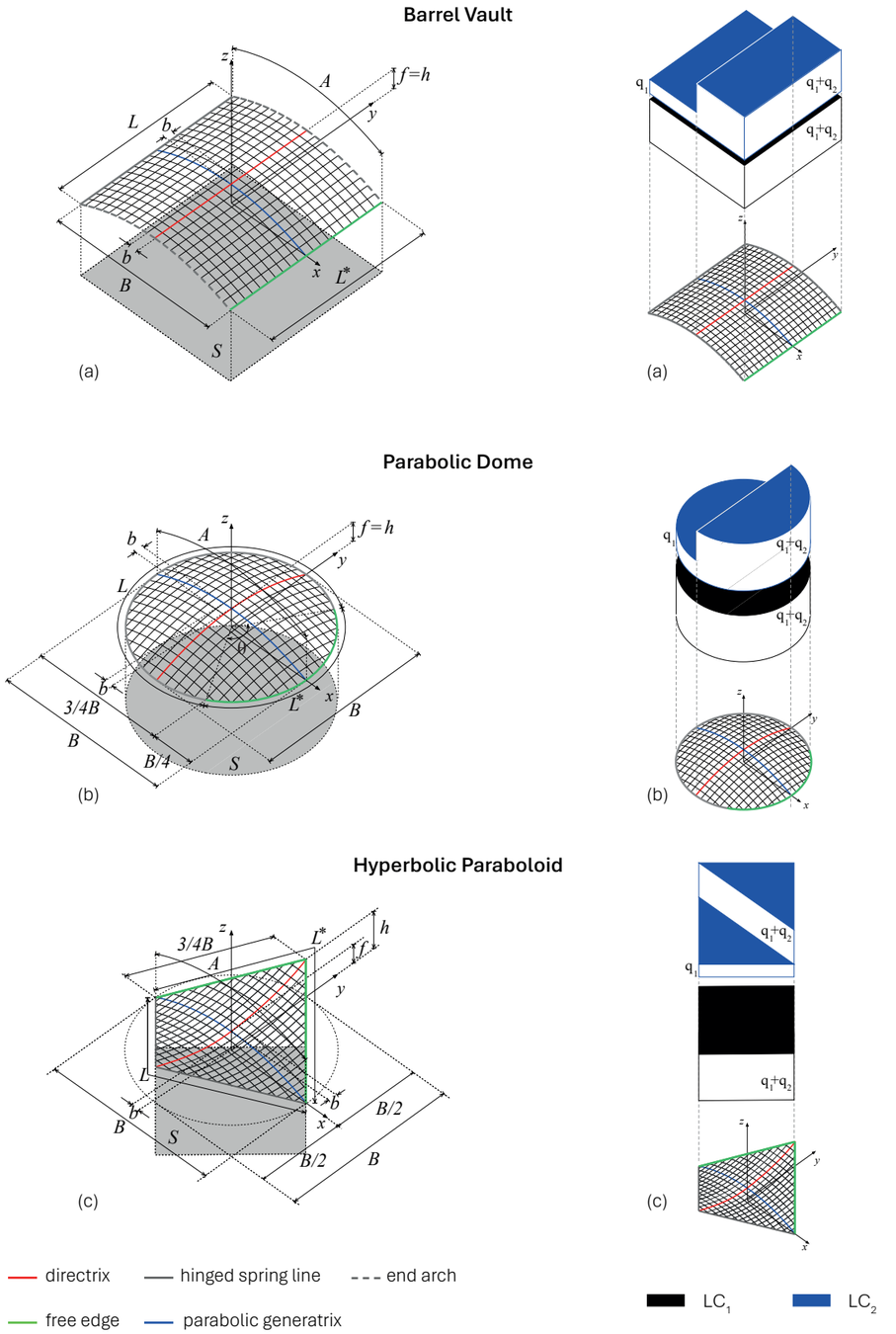

Figure 3.2: FreeGrid DBGs: barrel vault (a), parabolic dome (b), hyperbolic paraboloid (c)

Figure 3.3: Load Conditions for DBGs: barrel vault (a), parabolic dome (b), hyperbolic paraboloid (c)

and $y > 0$ for the hyperbolic paraboloid. Additionally, it includes point loads $Q_{2,2,k}=q_2 s_k$, where q_2 represents the uniformly distributed load, considering permanent weight of the glass, applied to the surface with $x < 0$ for the barrel vault and parabolic dome, and $y < 0$ for the hyperbolic paraboloid.
The values q_1 and q_2 differ for different assessments at ultimate limit state (ULS) and serviceability limit state (SLS) as outlined in Table 5.

	Description	ULS [N/m^2]	SLS [N/m^2]
g	self-weight of structural members	-	-
q_1	permanent weight of glass cladding	600	400
q_2	snow	1200	800

Table 5: Load values at ULS and SLS

Design Goals and performance metrics 3.4.0

Methodological framework 3.4.1

The geometrical and structural setups provided serve as a common foundation for all participants who are required to respect the guidelines set by the benchmark while developing their own proposals on the DBGs. The aim is to evaluate each solution from a holistic point of view, according to seven Design Goals DG.
The overall evaluation process for each proposed Design Solution Gridshells DSGs consists of three stages (Figure 3.4).
First, the Design Goals are expressed in the form of Goal Metrics, each associated with either an increase (↑) or decrease (↓) of the respective metric. Each metric is normalized (with asterisk '*') to a relevant characteristic of the gridshell or a specific design goal, allowing it to be compared with metrics from other solutions.
Then, the Design Goals and their corresponding Goal Metrics are gathered into three categories, representing structural performance (subscript 's'), buildability performance (subscript 'b') and sustainability performance (subscript 'su'), combined into partial performance metrics P_k, with k = *s*,*b*,*su*.

Finally, each partial metric is summarized into a global Bulk Performance metric *P* through a linear combination.
To ensure comparability, the partial metrics must be dimensionless, meaning that each value is compared to that of a reference solution (subscript '0'). The following formula expresses the linear combination of the dimensionless partial metrics, using weighting coefficients *γ*:

$$P = \gamma_s P_s + \gamma_b P_b + \gamma_{su} P_{su}$$

where $\gamma_s + \gamma_b + \gamma_{su} = 1$; $\gamma_s = \gamma_b = \gamma_{su} = 1/3$

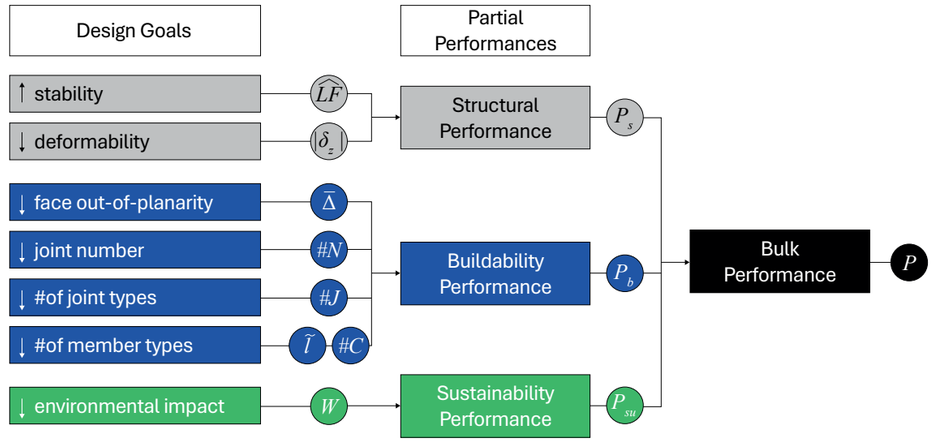

Figure 3.4: Evaluation process for DBGs and DSGs (Raffaele *et al*, 2024)

Structural performance 3.4.2

As previously stated, the design and optimization of their geometry must account for mechanical performances, in particular the potential for instability and deformability at both the ultimate limit state (ULS) and serviceability limit state (SLS). To evaluate these aspects, FreeGrid establishes specific metrics: Stability is assessed at the ULS, where gridshells failure mode affect their stability and strength. The reference metric considers local instability, global instability, element instability and/or the plasticization of structural members. It is represented by the Load Factor ($\widehat{LF}$) which is evaluated under load condition LC_1 e LC_2, with a lower threshold set at a normalized value of $\widehat{LF}_1$ =1.

Generally defined as $\widehat{LF} = Q_u/Q$, where Q_u is the magnitude of the ultimate load and Q is the design load under the reference load condition, the Load Factor is analitically defined in Figure 3.5. More precisely:

-the Load Factor corresponds to the minimum between LF_I (gridshell instability) and LF_P (full plasticization of at least one cross-section of a structural member);

-the ε^*_{min} and ε^*_{max} curves define the regime of instability in which LF falls. Specifically, ε^*_{min} = 1 represents the plasticization of at least one cross-section, while ε^*_{max} = 1 the plasticization of at least one fiber of a cross-section.

The elastic regime is defined by the condition ε^*_{min} , $\varepsilon^*_{max} < 1$ and $\varepsilon^*_{min} < \varepsilon^*_{max}$ defines elasto-plastic regime.

The condition ε^*_{min} , $\varepsilon^*_{max} > 1$ establishes a locally plastic regime and LF value is found at the intersection of ε^*_{min} curve with the threshold line $\widehat{LF}_1 = 1$;

-the condition $dLF/d\delta_z \leq K_1$ defines the tangent line, where the derivative $dLF / d\delta_z$ is nearly null.

Deformability is evaluated at the SLS by measuring the vertical displacement $|\widehat{\delta}|$ of the nodes under load conditions LC_1 and LC_2. The value must be reduced below the upper limit of $\widehat{\delta}_{z,l} = B/200$ (where B is the gridshell span), normalized as $\widehat{\delta}^*_{z,k} = \widehat{\delta}_{z,k} / \widehat{\delta}_{z,l}$.

The structural performance metric adopted by FreeGrid is averaged over K, i.e. load conditions LC_k, and it is defined as:

$$P_s = \frac{\sum_{k=1}^{K} \frac{\widehat{LF}_k}{\widehat{LF}_{k,0}} / \frac{|\widehat{\delta}^*_{z,k}|}{\widehat{\delta}^*_{z,k,0}}}{K}$$

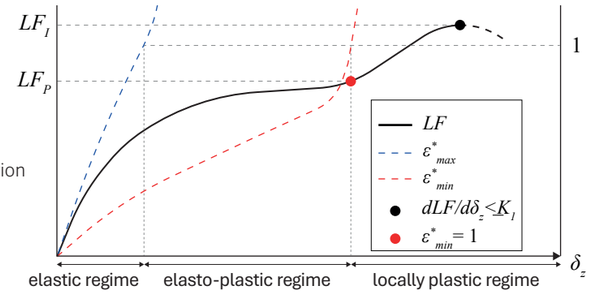

Figure 3.5: Structural performance: Load Factor definition criterion (Raffaele *et al*, 2024)

3.4.3 Buildability performance

FreeGrid introduces this metric to address performance related to fabrication-aware design which is not univocally and exhaustively defined in current literature. This is done according to a rigorous but not exhaustive approach that refers to: the geometry of 2D panels coincident with faces; the 1D structural members coincident with the edges; the 0D joint at vertices, while excluding the offset between panels and faces (as kinks of joints and edge offset).

FreeGrid defines the following Goal Metrics with respect to buildability.

First, the face out-of-planarity, a characteristics of double-curvature gridshells, that represents the limit to be overcome through the use of planar faces of the cladding panels, for reasons previously defined. The reference metric to be minimized is the average $\bar{\Delta}$, which is calculated based on every face, by taking the average of the distance between vertices of each face in approximation of the surface, then divided by the semi-perimeter length of the face.

The second metric refers to the number of structural joints and it is called #(N).

The third metric refers to the uniformity of joints, specifically the number of different types of them, that for FreeGrid is closely related to the valence of the joint v which indicates the number of converging members at that joint, as well as the relative angles θ between members. The metric to be evaluated is the number of joints typologies #(J), that is more favorable as it decreases.

The fourth metric concerns the uniformity of members, as well as the abacus of members used in the gridshell.

FreeGrid adopts the metric $\tilde{l}$ as the coefficient of length variations, and #(*C*) as the cardinality of the members cross-sections.
The partial performance metric is the average of the metrics previously defined, and it is described as:

$$P_b = \frac{1}{\frac{1}{5}\left[\frac{1+\overline{\Delta}}{1+\overline{\Delta}_0} + \frac{\#(N^*)}{\#(N_0^*)} + \frac{\#(J^*)}{\#(J_0^*)} + \frac{\#(\tilde{l}^*)}{\#(\tilde{l}_0^*)} + \frac{\#(C^*)}{\#(C_0^*)}\right]}$$

Sustainability performance 3.4.4

This metric is introduced into performance evaluation based on three motivations. First, the reduction of structural material, a traditional goal in structural design process, especially concerning lightweight structures. This focus supports the sustainable perspective of Life Cycle Assessment (LCA) as a topic relatively underdeveloped in the specific literature of gridshells.
FreeGrid merges structural and fabrication considerations in this metric by evaluating the environmental impact of the structural type of members cross-section and the steel grade used analogous to the embodied carbon coefficient, all within a single, comprehensive weighting parameter determined by the unit mass of elements.
The metric becomes increasingly favorable as the value decreases, and it is defined as:

$$P_s = \frac{1}{W^* / W_0^*}$$

where W^* is the parameter to be minimized, corresponding to the carbon consumption normalized with respect to the gridshell surface $\breve{S}$, and defined as:

$$W^* = \frac{W}{\breve{S}} = \frac{\sum_{i=1}^{M} g_i \, l_i \, \alpha_i}{\breve{S}}$$

where the summation over M structural members of the entire gridshell includes the weight per unit length g_i, the length of the i-th member l_i, and the environmental impact correction factor α_i, which depends on the steel grade and the cross-section type of the i-th member, normalized to the corresponding coefficient of the hollow section made of S355 steel. (Figure 3.6)

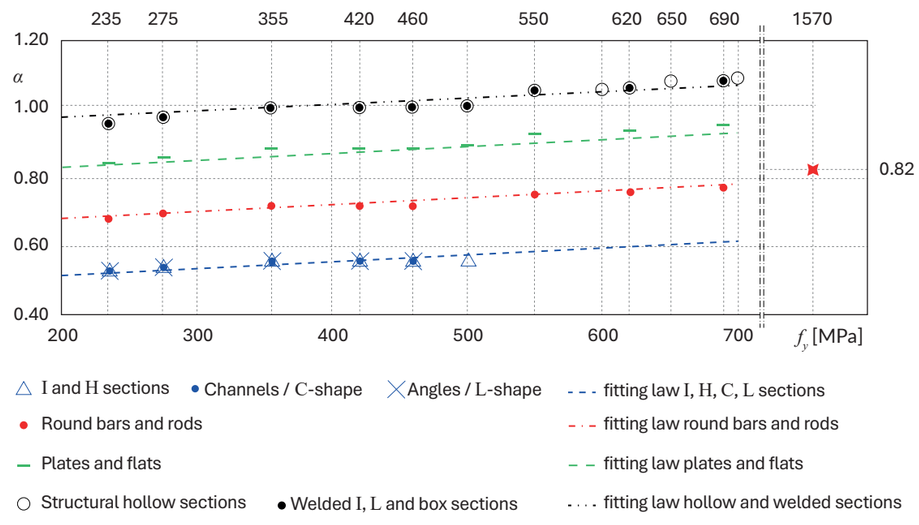

Figure 3.6: Sustainability performance: α parameter versus steel grade and type of member cross-section (Raffaele *et al*, 2024)

Table 6 reports all the Goal Metrics calculated for the three DBGs. Few considerations can be drawn within each partial performance metric by comparing the Design Goals among the three reference gridshells.
Based on the Structural Goal Metrics values, it can be observed that the three reference geometries are not significally affected by the two load conditions. Likewise, none of them achieve the performance thresholds at SLS and ULS established by FreeGrid, $|\widehat{\delta}| / \widehat{\delta}_{z,l} < 1$ and $\widehat{LF} > 1$ respectively. On the other hand, the variations in geometry lead to different structural performance at SLS, with the double-curvature DBGs (parabolic dome and hyperbolic paraboloid) exhibiting progressively higher performance. By contrast, the single-curvature barrel vault DBG proves to be approximately twelve times less stiff than the other two geometries, under both load conditions.
The comparison of the Buildability Goal Metrics across the DBGs highlights two commonalities shared by all three geometries. Each of them exhibits a unitary value in terms of face out-of planarity $1+\overline{\Delta}_0$ and cardinality of member cross-sections $\#(C_0)$, as a consequence of the geometric criteria previously defined.
The highest joint number $\#(N_0)$ belongs to the barrel vault DBG, considering the normalization with respect to its surface

-which is the larger-. Nevertheless this, the barrel vault DBG is the most homogeneous in terms of uniformity of structural joints #(J_0), as its boundaries are aligned with the surface grid. Regarding uniformity of structural members, the barrel vault DBG scores a unitary value also for member length $1+\tilde{l}_0$. As a matter of fact, it is the only geometry where all elements share the same length, due to its fully quad mesh pattern. By contrast, the other DBGs show increasing values due to the presence of triangular cells.
The Sustainability Goal Metric is significantly more demanding for the barrel vault DBG. Its high value stems from the larger cross-section area of the elements used, which is twice that of the one in the other DBGs, resulting in a higher normalized equivalent weight.

	Structural Goal Metrics				Buildability Goal Metrics					Sustainability Goal Metric
Reference DBG	$\widehat{LF}_{0,1}$ [-]	$\lvert\widehat{\delta}_{z,\theta 1}\rvert$ [m]	$\widehat{LF}_{0,2}$ [-]	$\lvert\widehat{\delta}_{z,\theta 2}\rvert$ [m]	$1+\bar{\Delta}_0$ [-]	$\#(N_o)$ [-]	$\#(J_o)$ [-]	$1+\tilde{l}_0$ [-]	$\#(C_o)$ [-]	W_o [kg]
Barrel vault	0.833	1.793	0.871	1.824	1	441	4	1	1	57556
Parabolic dome	0.802	0.359	0.805	0.351	1	377	25	1.194	1	23564
Hyperbolic paraboloid	0.769	0.175	0.781	0.176	1	257	13	1.225	1	15589

Table 6: DBGs Structural, Buildability and Sustainability performance metrics

3.5.0

Design Constraints

FreeGrid establishes Geometrical Constraints (GC) and Mechanical Constraints (MC) that participants are required to observe in their design proposals for each Design Solution Gridshell (DSG). These constraints are outlined below, as described in the technical specifications of the benchmark (Bruno *et al*, 2023-e).

Geometrical Constraints:
GC1 the single-layer gridshell structural type cannot be changed, i.e., the mesh is 2-manifold, that is, non-manifold vertices and edges are not permitted;
GC2 the position, shape and length of the continuous spring line and of the head arches (for barrel vault only) cannot be modified;
GC3 the gridshell spans along the *x* and *y* directions B_x and B_y, respectively, shall not be shorter than 30 m, being B_x and B_y generally defined as the maximum span free of external constraints;
GC4 the extent of the projection of the overall gridshell surface on the horizontal reference plane shall be no smaller than S−0.05S ;
GC5 the rise shall be kept equal to *f*=*B*/8, being *f* generally defined as the distance between the horizontal reference plane and the horizontal tangent plane to the shell surface having the minimum height;
GC6 the height h shall be no longer than *b*/4, being h generally defined as the distance between the horizontal reference plane and the horizontal plane passing through the shell vertex having the maximum height;
GC7 geometrical vertices and structural joints cannot lie below the horizontal reference plane;

Mechanical Constraints:
MC1 along the spring line *L*, *x*-, *y*- and *z*-displacements of all the structural joints resulting from mesh generation shall be externally constrained (perfect hinges);
MC2 along the head arches (barrel vault), *x*- and *z*-displacements of all the structural joints resulting from mesh generation shall be externally constrained;
MC3 additional structural external constraints are not allowed

anywhere;
MC4 the structural members shall have commercial cross sections;
MC5 the structural material shall be steel.

The variation of any parameter is permitted unless explicitly excluded by the aforementioned limits. The design and optimization approach can be various, including man-based heuristic methods or artificial intelligence (e.g. neural networks, machine learning), gradient-based or topological design, physical scale models, or continuous analogy models for optimization. It is allowed any types of structural modeling, with the requirement that the final structural performance evaluation of the DSGs must be carried out through a Geometrically and Materially Nonlinear Analysis (GMNA).

FEM Specifications

3.6.0

For the evaluation of Partial Metrics and the overall performance of the gridshells mechanical behaviour, Freegrid establishes specific technical requirements regarding the computational model to ensure the comparability of results across different FEM models. The guidelines address the Governing Equations, FEM discretization and Numerical Solver.

Governing Equations:
-the GMNA (Geometrically and Materially Non-linear Analysis) is performed considering the perfect structure without geometric imperfections. The adoption of this model allows the evaluation of the structure in terms of interaction between strength capacity and buckling and plasticity failure under large displacements (Raffaele et al, 2024). In the present study, the GMNA is carried out using the Finite Element code ANSYS® Mechanical APDL;
-the material should be modelled with an elastic-perfect plastic behaviour;
-a Distributed Plasticity model with nonlinear behaviour along the element and across its cross-section is recommended to follow the progressive yielding of members. For comparison purposes, a Concentrated Plasticity approach is also

implemented with specifications. These regard the positioning of plastic regions at the nodes and their length, being double the maximum cross-sectional dimension of each member.

FEM Discretisation
-finite elements should be modelled as cubic two-nodes beams, according to the Timoshenko theory, with 6 degrees of freedom per node and three points of integration along their longitudinal development;
-each structural member should be discretized into four Finite Elements to simulate local instability arising from second order effects.

Numerical Solver:
-load control must be applied in the incremental analysis with a load step magnitude of LC/1000 for each load step, where LC is the magnitude of the corresponding load condition;
-iterations must achieve convergence at each load step using the standard Newton-Raphson method, with a tolerance of 5e-3 for weighted residuals of the variables during the preliminary phases, and then declared by participants.

The Barrel Vault FreeGrid Design Baseline Gridshell **3.7.0**

The present research focuses on the Barrel Vault Design Baseline Gridshell (Figure 3.7) which stands out as the least efficient among the three DBGs. Indeed, the analysis of the partial metrics reveals that its structural performance is the weakest, with a maximum displacement at Serviceability Limit State approximately twelve times greater than the threshold displacement (Bruno *et al*, 2023-a).

The Barrel Vault DBG exhibits the geometrical characteristics described in Section 3.2. Its single curvature, as opposed to the double curvature seen in the other two DBGs, is what distinguishes this study case as more challenging than the other two geometries. The free-edge lies in the direction of zero curvature, i.e. it follows a horizontal line, unlike in the other two DBGs.

The structural characteristics, also defined earlier, indicate that the Barrel Vault DBG features members with a 139.7 mm diameter and 14 mm thickness, unlike the other two DBGs which share the same cross-section elements.

As already stated, another structural aspect unique to the Barrel Vault DBG lies in the boundary conditions of the head arches, which are allowed to translate along *y*-axis.

Structural analysis

The structural behaviour of the DBG was evaluated through a 3D Finite Element Model based on the benchmark settings outlined in section 3.6. As previously stated, the GMNA analysis was conducted by the Ansys Mechanical APDL code to assess the structural performance at ULS and SLS under two load conditions. Each finite element was assigned an element type called 'BEAM188' in the software, which corresponds to a Timoshenko beam (Ahmed and Rifai, 2021).

The ULS analysis assessed the stability of the DBG giving back as output the load-displacement curve (Figure 3.8) for both load conditions LC_1 and LC_2. This analysis has shown that:

-the mechanical behaviour of the DBG is not strictly dependent on the load condition, as the curves corresponding to both LC_1 and LC_2 reach similar critical load values (*LF*). These values are $LF = 0.833$ for LC_1 and $LF = 0.871$ for LC_2. Therefore, in both cases, the lower bound set by FreeGrid $\widehat{LF}_1 = 1$ is not

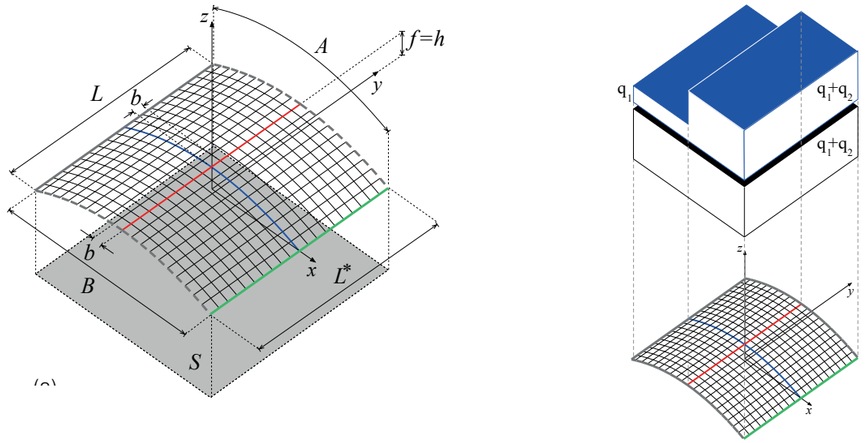

Figure 3.7: DBG barrel vault: geometry and load conditions

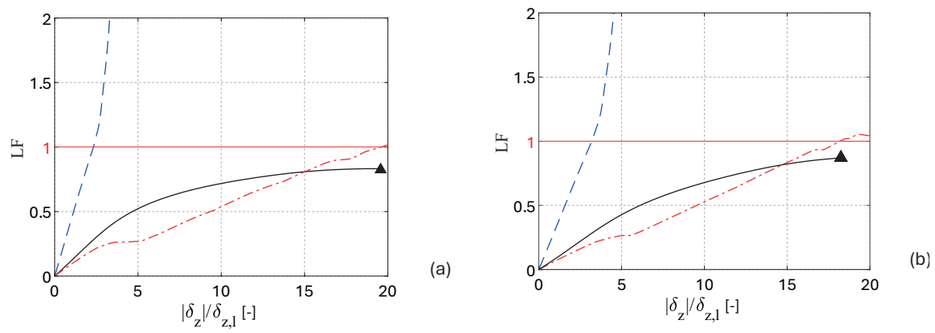

Figure 3.8: Load-displacement curves in LC_1 (a) and LC_2 (b)

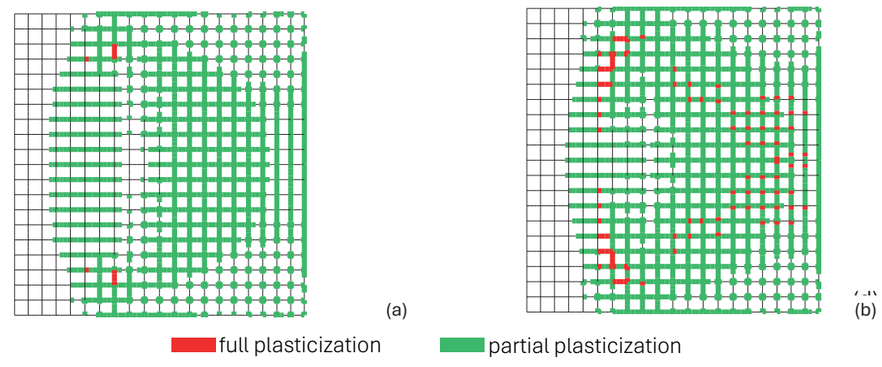

Figure 3.9: Yielded FE in LC_1 (a) and LC_2 (b)

satisfied. By contrast, the mechanical behaviour of fully-constrained barrel vault is significantly influenced by different load conditions applied (Raffaele *et al*, 2024);
-the ULS is reached due to the full plasticization of one or more members under both load conditions (Figure 3.9), as both ε^*_{min} and ε^*_{max} curves exceed 1. The identification of the Load Factor occurs in a locally-plastic regime, due to development of plastic hinges before reaching global instability (buckling phenomenon). Conversely, the Load Factor of fully-constrained barrel vault falls in a elastic regime for LC_1 and elasto-plastic regime for LC_2 (Raffaele *et al*, 2024), therefore global instability occurs in both cases without full plasticization of cross-sections.

The SLS analysis assessed the deformability of the DBG by evaluating the maximum normal and tangential displacements of the joints (Figure 3.10). The results summarized in Table 7 show that both normal ($\hat{\delta}_\perp$) and tangential ($\hat{\delta}_{//}$)displacements are significant in magnitude, being the normal component predominant.
The maximum normal component is higher under load condition LC_2, while the maximum tangential one is higher in LC_1. In both load conditions, maximum normal (Figure 3.10-a) and tangential (Figure 3.10-b) displacements are concentrated in the surface around the free-edge and increase along the arches in the positive *x*-axis. Similarly, the peak displacement pattern remains unvaried across both load conditions. This further confirms that varying load conditions do not significantly affect the mechanical behaviour of the DBG, since the free-boundary effects are prevailing with respect to the asymmetric loading effects. As with LF, in the displacement evaluation the free-edge plays a decisive role in determining the displacement patterns, unlike the fully-constrained barrel vault, where different load conditions result in different patterns (Raffaele *et al*, 2024).

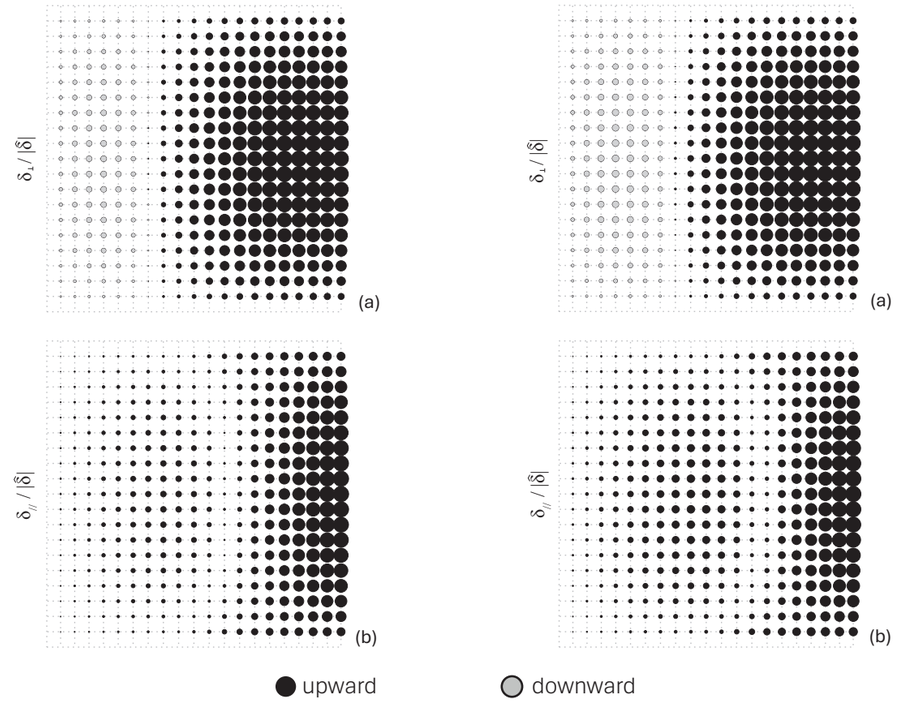

Figure 3.10: Normal (a) and tangential (b) displacements in LC_1 (fist row) and LC_2 (second row)

	$\hat{\delta}_\perp$ [m]	$\hat{\delta}_{//}$ [m]	$\delta_\perp / \hat{\delta}_{z,I}$
Load Condition LC_1	1.793	0.501	11.95
Load Condition LC_2	1.824	0.435	12.16

Table 7: normal and tangential displacement maximum values in LC_1 and LC_2

The effects of DBG deformability at SLS are presented in Figure 3.11 in terms of out-of-plane and in-plane nodal deformations. Figure 3.11-a shows the out-of-plane behaviour of the DBG by evaluating the difference between the deformed and undeformed configurations of the discrete Gaussian curvature $\Delta k=k-k_0$. Figure 3.11-b represents the in-plane behaviour through the equivalent shear deformations $\Gamma = \gamma_{xy}(pN) + \gamma_{xy}(p\varepsilon)$, of each quadrangular cell (Raffaele *et al*, 2024) (Figure 3.12).

It is evident that, under both symmetric and asymmetric load conditions, the out-of-plane deformations are significant and concentrated in the surface area between the maximum rise and the free-edge, where $\Delta k<0$. The maximum in-plane deformations occur around the free-edge supports instead.

Within the same limit state analysis, the DBG behaviour was evaluated under the most unfavorable load condition, LC_2. Contrary to the characteristic behaviour of gridshells, the results demonstrate the prevalence of bending moments over the membrane behaviour, as shown in Figure 3.13.

Figure 3.13-a represents the normalized distribution of axial forces $N^*=N / |\widehat{N}|$, where $|\widehat{N}|$ is the DBG maximum axial force in LC_2. It reveals that members along the free-edge are under tension, with higher axial force levels compared to the other members. The same figure shows a predominance of axial compression along members in the y-axis direction, which are concentrated close to the maximum rise of the gridshell.

Figure 3.13-b shows the distribution of the resulting normalized bending moment moduli $M^*=M / |\widehat{N}|b$, which reveals that the onset of bending moments affects a significant portion of DBG members. Specifically, the asymmetric load condition produces greater bending moments in the elements aligned with the *x*-axis, particularly within the surface domain between the constrained edge and the maximum rise. On the other hand, the bending moments in the *y*-direction members are of lower magnitude. In the region between the line of maximum rise and the free-edge, the bending moments in *y*-axis members maintain similar magnitude as previous, while increase for those along *x*-axis.

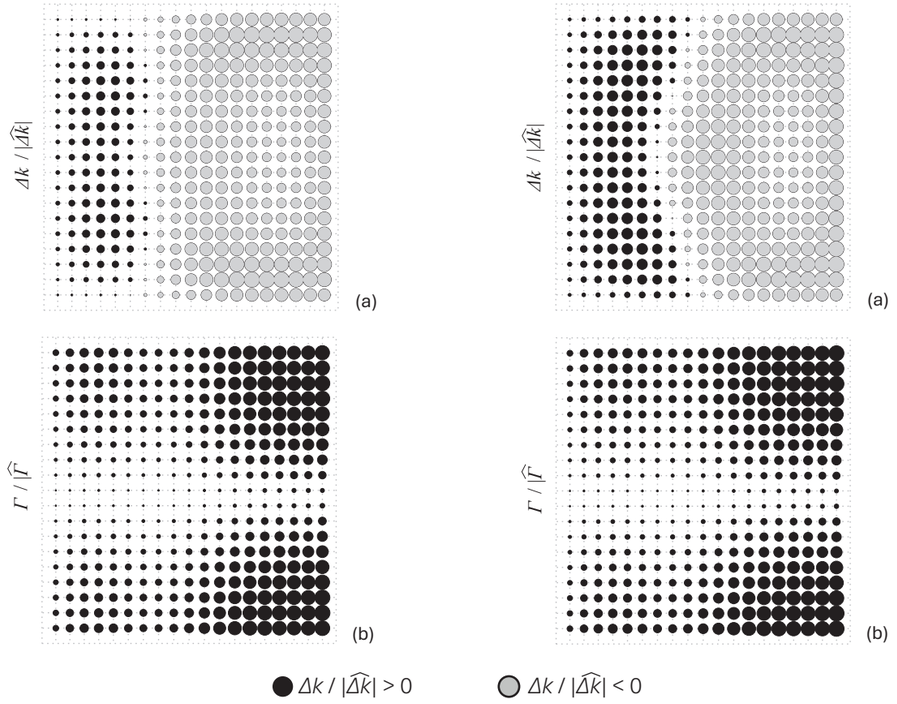

Figure 3.11: Out of plane (a) and in plane deformations (b) in LC_1 (first row) and LC_2 (second row)

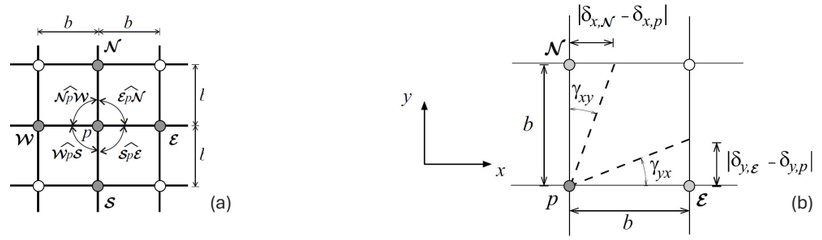

Figure 3.12: Schemes for the definition of discrete gaussian curvature (a) and equivalent shear deformation (b) (Raffaele *et al*, 2024)

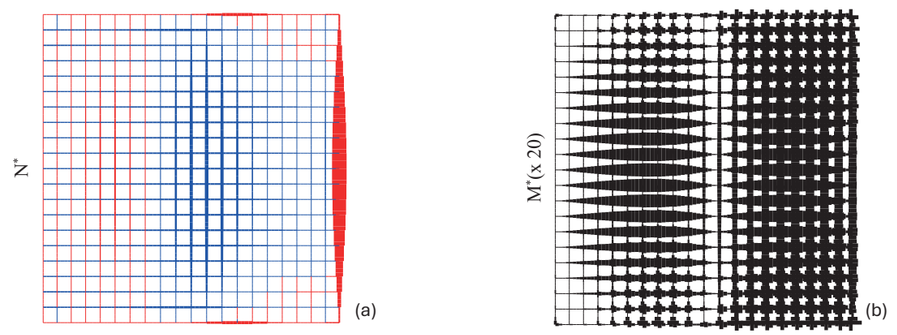

Figure 3.13: Normalized distribution of axial forces (a) and distribution of resulting bending moments (b)

Chapter

4

Proposals of Design Solution Gridshells

Based on the mechanical behaviour of the DBG reported by the load factor *LF* and the maximum nodal displacement $|\widehat{\delta}|$ for both load conditions, Design Solution Gridshells primarily aim to improve structural performance. Therefore, they seek to exceed the lower bound of the critical load factor $\widehat{LF}$ = 1 and keep the maximum displacement within the upper limit of $\widehat{\delta}_{z,l}$ = B/200 = 0.15 m set by FreeGrid

Secondly, all the proposed design solutions aim to minimize modifications to the DBG geometry by limiting the number of additional members and the different size of their cross-section. This means the proposed DSGs share the same number of joints and their coordinates with the DBG, even though the type of joints should necessarily increase due to the addition of structural members to the grid. The latter issue does not play a secondary role as any modifications to the original DBG geometry could worsen Buildability and Sustainability partial metrics in spite of improvements in the structural performance metric, thereby reducing the overall performance represented by the bulk metric. In other words, a DSG with superior structural performance but lower buildability and sustainability ones might achieve a worse overall performance than another DSG with lower structural performance but better values of buildability and sustainability metrics.

The proposed DSGs comply with the benchmark criteria and share the common goal of restoring the membrane behaviour of the gridshell, favoring the overall structural conception rather than prioritizing the sizing of each member.

Design references

4.1.0

The structural design strategy adopted for the DSGs follows a common approach known in literature as design from precedent (Boling, 2021), which involves drawing inspiration from similar, previously conceived solutions.

In this study, few solutions are selected from real-world design of single-layer steel gridshell as well as other exemplary cases, which are used as references and developed in analogy with the problem statement.

The first strategy takes into account the increase of the cross-section size of members along the free-edge L^* to locally

control it by providing the members with sufficient flexural and torsional stiffness (Bruno *et al*, 2024). This strategy is seen, for instance, in the design of the Bristol Cabot Circus, by Schlaich Bergermann und Partner (Schober and Justiz, 2012) (Figure 4.1).

The second approach aims to triangulate the original quad mesh by introducing diagonal, stabilizing members within each grid unit. The purpose of this solution is to enhance the membrane stiffness and, consequently, reduce in-plane shear deformations of the cells (Bruno *et al*, 2024) as exemplified in the House for Hippopotamus in Berlin conceived by the same designers as the previous reference (Schlaich and Schober, 1997) (Figure 4.2).

As a third approach, the research for free-edge stiffness takes into account the use of a truss-girder inspired by hangars projects designed by Pier Luigi Nervi (Leslie, 2018), where the concrete structure is stiffened with a spatial truss-girder along the free-edge spring lines (Figure 4.3).

Finally, a last strategy is taken from an uncommon solution for gridshells design, rooted in traditional masonry barrel vaults instead. This solution sees a relieving arch laid on the surface which role is to redirect the thrust forces, transferring them towards the lateral constraints rather than relying on the free-edge (Figure 4.4).

Conceptual design

4.2.0

The references previously discussed have been reinterpreted and adapted into the following Design Solution Gridshells outlined in Figure 4.5.

DSG A (Figure 4.5-a) retains the same number of structural members and consequently the same type of joints as the DBG but differs in the structural characteristics of the members along the free-edge. As in the first reference, the diameter of these elements is increased following the typical design criteria for single-layer, quad mesh pattern gridshells. The assigned elements have a circular cross-section with a diameter of 610 mm and a thickness of 16 mm, whose inertia is about 120 times greater compared to the cross-section used for the DBG elements.

DSG B (Figure 4.5-b) applied the second approach mentioned, by inserting a diagonal member in each cell of the grid with the same cross-section as the DBG members. This strategy results in the change of valence v of most joints as compared to the DBG ones, caused by the increased number of members converging at a joint. Consequently, it increases the variety of joints types #(*J*) due to the different orientation of the added diagonals.

DSG C (Figure 4.5-c) is inspired by the strategy derived from the insertion of a truss-girder, as mentioned in the third reference, but its advantages are limited by constraints imposed by the benchmark. Actually, the added diagonal members forming the truss-girder must necessarily lie on the surface of the vault, excluding the presence of non-manifold vertices and edges. This restriction, which excludes the use of spatial truss-girder, limits this strategy to improve only the in-plane stiffness. The added elements share the same cross-section as those of the entire grid. They control the free-edge across the first two cell levels, adhering to the conventional preliminary dimensional design for trusses, for which the height is approximately 1/100 of the span. For the same reason mentioned before, the joint types and valence vary from those of the reference gridshell.

The proposed DSGs in category D take as a reference the final strategy outlined in Chapter 4.1 (Figure 4.5-d) and develop multiple solutions divided into three subcategories (relieving arches, flying buttresses, relieving arches and flying buttresses) (Figure 4.5-e, f, g). The aim is to assess the gridshell performance under different combinations.

For all DBGs in this category, the added members share the same cross-section as those in the DBG and, once again, variations in joint types and valence are expected.

Figure 4.1: Cabot Circus, Schlaich Bergermann und Partner (Bristol, 2008)

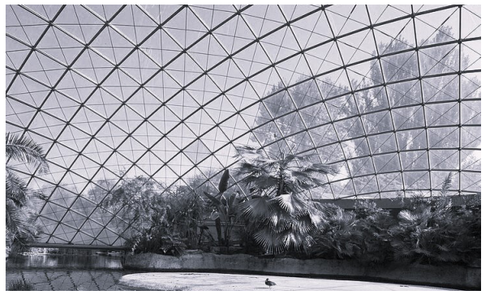

Figure 4.2: House for Hippopotamus, Schlaich Bergermann und Partner (Berlin, 1996)

Figure 4.3: Example of Pier Luigi Nervi Aircraft Hangar

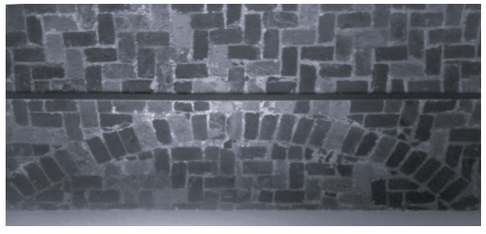

Figure 4.4: Example of strategy for masonry vault

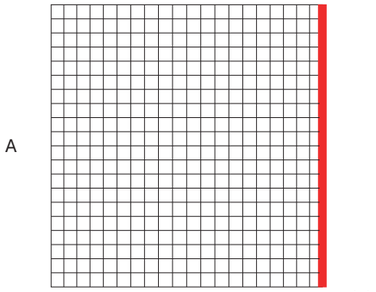

Figure 4.5: Schemes of Design Solution Gridshells (a; b; c; d)

In category D1(Figure 4.5-e), the proposed solutions assess the effect of varying the rise of the arch lying on the surface of the gridshell. D1.1 and D1.2 (Figure 4.5-e.1,2) feature a single relieving arch with a rise *r* equal to *L*/4. They differ in the way the curves have been discretized;
D1.3 (Figure 4.5-e.3) presents two relieving arches, symmetrical around *y*-axis, with the rise *r* equal to *L*/4 and -*L*/4;
D1.4 (Figure 4.5-e.4) shows a relieving arch with a rise *r* equal to *L*/2;
D1.5 (Figure 4.5-e.5) includes a relieving arch with a rise *r* equal to 3*L*/4;
D1.6 (Figure 4.5-e.6) features a pair of relieving arches with rises *r* equal to *L*/4 and *L*/2, respectively.

In category D2 (Figure 4.5-f), the solutions explore the gridshell behaviour under the effect of two added flying buttresses-like, also lying on its surface.
D2.1 (Figure 4.5-f.1) features flying buttresses-like with their maximum vertex at the midpoint of the free-edge;
D2.2 (Figure 4.5-f.2) combines the same flying buttress-like configuration with a relieving arch having rise *r* equal to *L*/4;
D2.3 (Figure 4.5-f.3) pairs the flying buttresses-like with a relieving arch having rise *r* equal to *L*/2;
D2.4 (Figure 4.5-f.4) presents flying buttresses-like with their maximum vertex at -3*L*/4, combined with a relieving arch with rise *r* equal to L/4.

In category D3 (Figure 4.5-g), the proposed solutions aim to analyze the combined effect of relieving arches and flying buttresses that intersect at varying points, anchored at the ends of the constrained edges. In this case as well, the added elements maintain the cross-section of the original structural members while inserting variability in joint types and valence.
D3.1 (Figure 4.5-g.1) combines two flying buttresses, symmetrical around *x*-axis, with a relative distance d equal to 4*b* (Figure 4.6-a) and trimmed at the intersection with a relieving arch having rise *r* equal to *L*/4;
D3.2 (Figure 4.5-g.2) presents a similar configuration but with a relative distance d equal to 6*b* (Figure 4.6.b), while still trimmed by a relieving arch with rise *r* equal to *L*/4;

D1 - relieving arch (e)

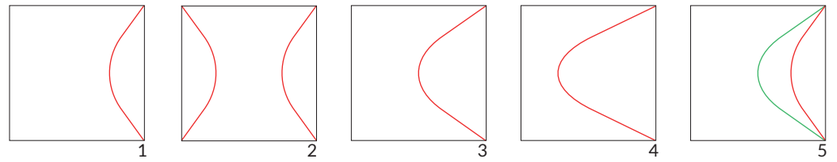

D1	D1.1 - D1.2	D1.3	D1.4	D1.5	D1.6
r_1	L/4	L/4	L/2	3L/4	L/4
r_2	-	-L/4	-	-	L/2

D2 - relieving arch and flying buttress-like (f)

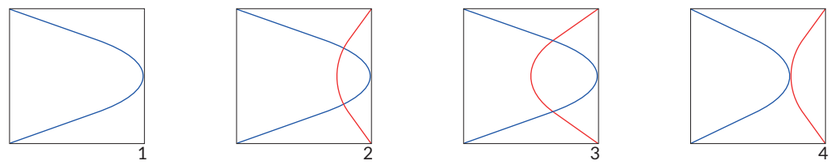

D2	D2.1	D2.2	D2.3	D2.4
r	-	L/4	L/2	L/2
f	-L	-L	-L	-3L/4

D3 - relieving arch and flying buttresses (g)

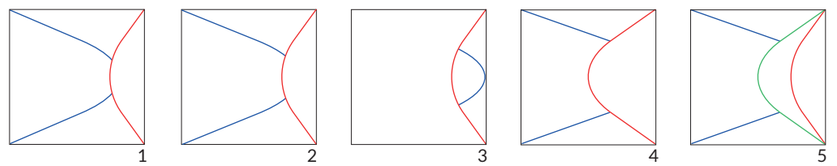

D3	D3.1	D3.2	D3.3	D3.4	D3.5
r_1	L/4	L/4	L/4	L/2	L/4
r_2	-	-	-	-	L/2
d	4b	6b	10b	10b	10b

Figure 4.5: Schemes of Design Solution Gridshells (e; f; g)

D3.3 (Figure 4.5-g.3) has the same configuration as D2.2 but the portion between the constrained edge and the arch is trimmed. The aim of this solution is to test the combination of arch and flying buttresses-like;
D3.4 (Figure 4.5-g.4) increases the relative distance between the flying buttresses equal to 10*b* (Figure 4.6-c), trimmed at the intersection with a relieving arch with a rise *r* equal to *L*/2;
D3.5 (Figure 4.5-g.5) follows the same configuration as D3.4 but adds a second relieving arch with a rise *r* equal to *L*/4.

All the proposed solutions in D category have been geometrically defined through a discretization criterion, whereby each curve defining arches and flying buttresses is broken down into segments converging at the nodes of the involved grid cells. Each added element, therefore, represents an approximation of the curve, as demonstrated in Figure 4.7.

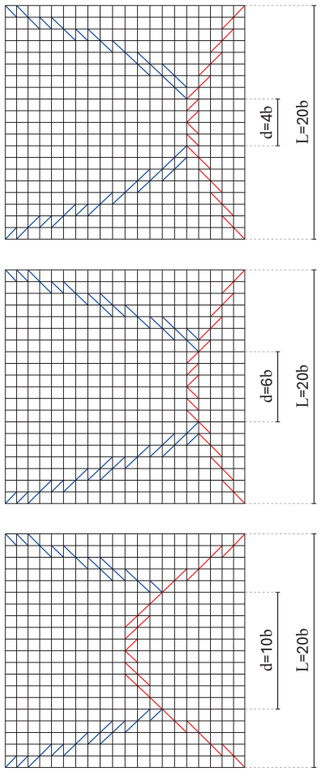

Figure 4.6: Schemes of relative distance between flying buttresses and arches

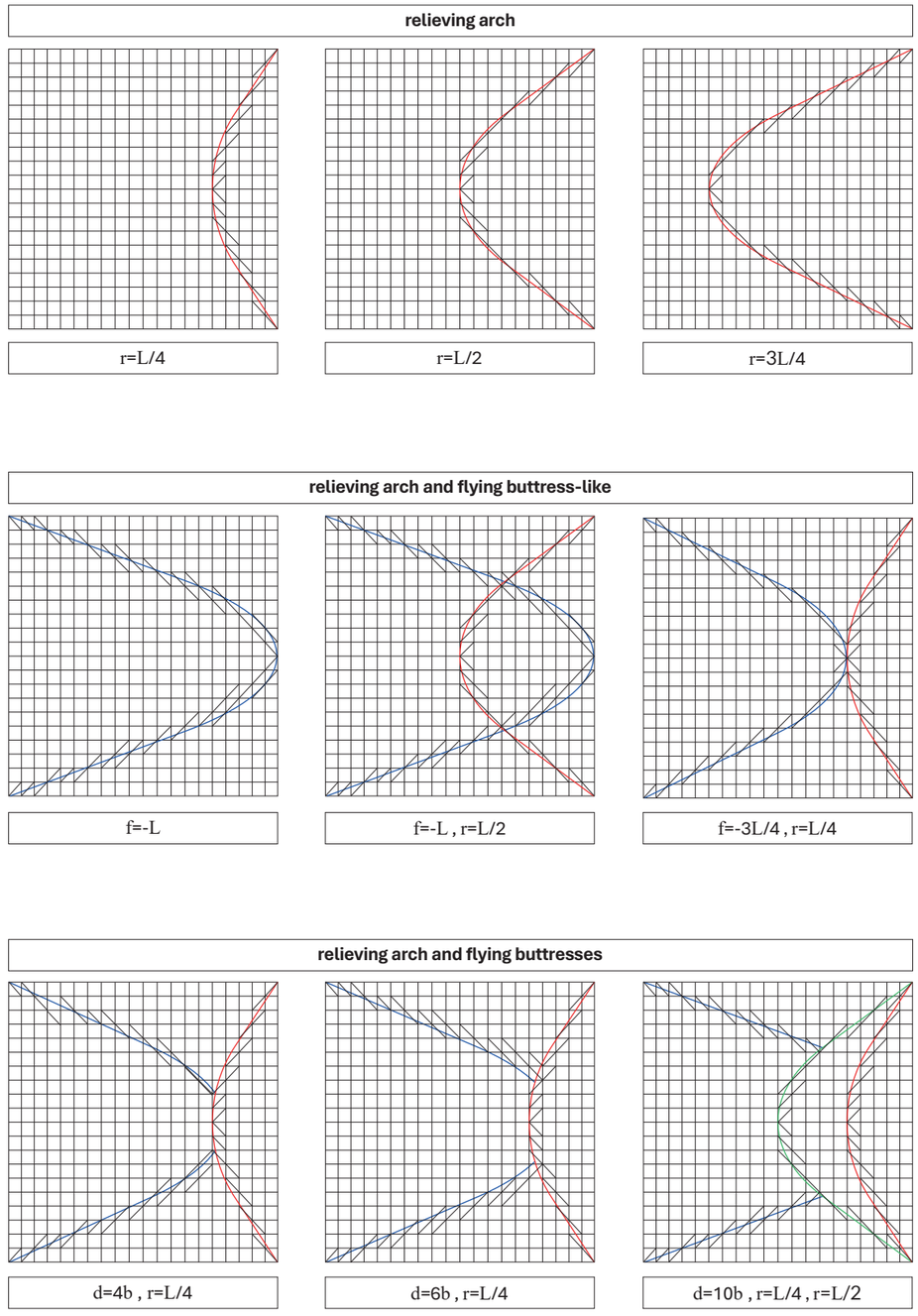

Figure 4.7: Schemes of discretization of arches and flying buttresses

Preliminary analyses **4.3.0**

As previously stated, the DSGs were compared in terms of mechanical behaviour to primarily evaluate their Structural Performance. In Figure 4.8 the ULS behaviour of each proposed solution is summarized under both load conditions. Specifically, the load-displacement curves are grouped according to DSG type, as classified in section 4.2.

The comparison assesses the effects of geometric variations for each category in relation to DBG behaviour. Moreover, each load-displacement curve provides data regarding partial (symbol●) or full (symbol▲) plasticization of the grid members.

Critical Load Factors are collected in Figure 4.9, together with normalized maximum displacements at SLS.

Figure 4.8-a compares the load-displacement curves of DSGs categories A, B, C with the DBG. It highlights that, under both load conditions, the quad-mesh (DBG) and triangular grid (B) represent the lower and upper boundary curves, respectively.

DSG A does not exhibit sufficient stiffness, even with larger cross-section of members along the free-edge. This is particularly evident under asymmetric load condition, where the gridshell reaches ULS due to the full plasticization of one or more members.

DSG B successfully exceeds the Load Factor threshold but lacks sufficient out-of-plane stiffness ($|\widehat{\delta}_z| / \widehat{\delta}_{z,l} = 2.5$).

DSG C is effective in reducing in-plane deformability but fails to address out-of-plane deformability, as $|\widehat{\delta}_z| / \widehat{\delta}_{z,l} > 10$. This issue stems from the impossibility of configuring a spatial truss-girder according to benchmark constraints. Therefore, the effectiveness of this solution is compromised when subjected to out-of-plane strain.

Figure 4.8-b shows the load-displacement curves for DSGs category D1, comparing the mechanical behaviour in response to variations in the rise of the relieving arch. The curves point out that the effectiveness of the relieving arch occurs when the rise *r* is less than *L*/2. As a matter of fact, a comparison of D1.1 (*r* =L/4), D1.4 (*r* =L/2) and D1.5 (*r* =3L/4) shows that the latter exhibits a higher critical Load Factor but also significant displacements, able to reach ULS due to full plasticization in LC_2. Moreover, as the rise decreases, geometric stiffness increases and displacements reduce, in particular

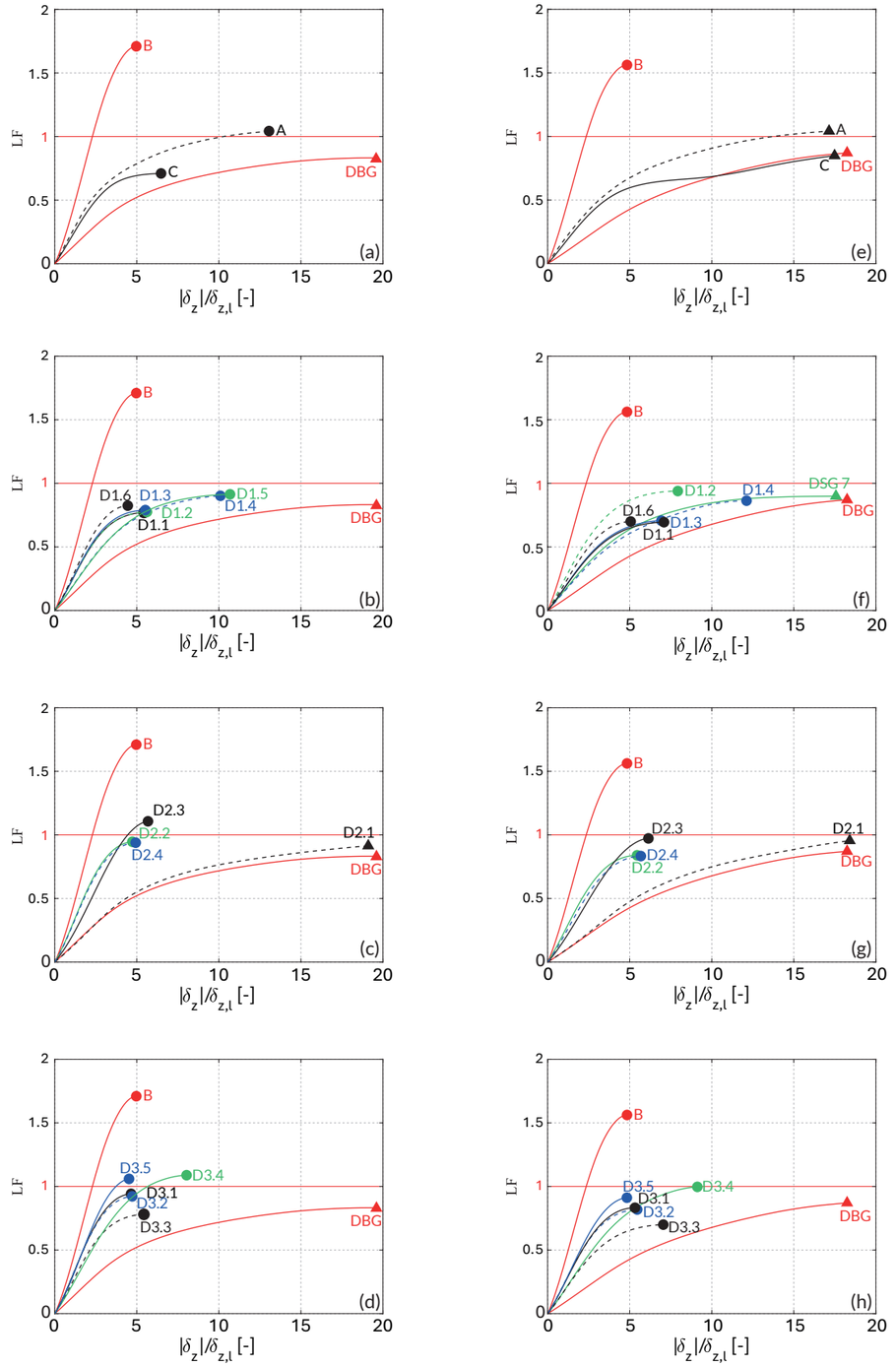

Figure 4.8: Load-displacement curves in LC_1 and LC_2

for D1.6 where arches with *L*/4 and *L*/2 rise are combined. On the other hand, a lower rise leads to higher concentration of internal forces in the arch and lower critical Load Factors, which brings forward global instability. This issue becomes more critical as the rise of the relieving arch increases, where instability is reached at larger ultimate displacements despite higher critical load values.

A final consideration can be made regarding the three different geometric configurations D1.1 (arch with *r*=L/4), D1.2 (arch with *r*=*L*/4, different discretization) and D1.2 (pair of arches with *r*=*L*/4 and *r*=*L*/2): their load-displacement curves are nearly analogous. This means that the addition of a symmetric relieving arch and changes in discretization do not enhance effectiveness.

Figure 4.8-c shows the load-displacement curves for DSGs category D2, it assesses the mechanical behaviour related to the addition of flying buttresses-like and its combination with relieving arches of varying rises.

D2.1 curve shows that the flying buttress-like alone is unable to achieve any structural goals, its behaviour is similar to the DBG for both load conditions. However, the combined effect of flying buttress-like and arch is effective under both LC_1 and LC_2. Once again, arches with rise greater than *L*/2 prove ineffective, as the load-displacement curves for D2.2 and D2.4 are nearly overlapping. Conversely, the solution with rise equal to *L*/2 (D2.3) is more effective.

More broadly, the addition of flying buttresses-like combined with relieving arch of varying rise, exhibits its effectiveness in reducing displacements (comparison between D1.1-D2.2, D1.4-D2.3). In spite of that, displacements remain significant ($|\widehat{\delta}_z| / \widehat{\delta}_{z,I} \approx 5$) , due to out-of-plane displacements beneath the relieving arch. Furthermore, the flying buttress-like enhances both stiffness and critical Load Factor of the DSGs, while tracing back members to partial plasticization.

Figure 4.8-d presents the load-displacement curves for DSGs in category D3. The choice to trim the flying buttress-like where it intersects the relieving arch was made to assess the active-effect of this strategy. A comparison between D3.2 and D2.2 reveals that both solutions exhibit similar behaviour, because of members almost inactive beneath the relieving arch.

Further evidence for this can be observed by comparing the D3.2 and D3.3 load-displacement curves. The one belonging to a relieving arch with rise of *L*/4 combined with flying buttress-like between the arch and the free-edge, coincides with D1.1 curve (relieving arch with *r*=L/4). This demonstrates that the flying buttresses-like are ineffective in bearing loads.

The analysis also takes into account the effect of the distance d at which flying buttresses intersect relieving arches. As shown by the comparison between D3.1 and D3.2, the effect is negligible. As a result, this latter comparison suggests that the role of flying buttress is not to alter the effective length of the relieving arches, but rather to limit their out-of-plane displacements.

Moreover, D3 category solutions achieve the design goal of redirecting the gridshell toward a membrane behaviour, as highlighted by the fact that ULS is reached due to global instability in quasi-elastic regime. These solutions are also marked by reduced displacements and increased critical Load Factor values, especially in D3.5 where the flying buttresses are combined with two relieving arches having rise equal to *L*/4 and *L*/2.

In general, several observations can be drawn regarding the load-displacement curves and values of critical Load Factor and normalized displacements (Figure 4.9). The following points can be noted:

-the curves of DBG and DSG B represent the range within which all DSGs load-displacement curves fall. This justifies the selection of DBG and DSG B as reference cases;

-all proposed DSGs contribute to an increase in the tangent stiffness of the DBG. Furthermore, the majority of the curves either approach or exceed DSG A stiffness, which was conceived as a stiffened edge beam solution;

-the load condition LC_2 is more demanding than LC_1. As a matter of fact, the solutions exhibit lower critical Load Factor values for this load condition and the plasticization shifts from partial to full in some cases (A, C, D1.5);

-most solutions do not achieve complete plasticization, resulting in ULS being reached due to global instability, as opposite to the DBG;

-besides the reference DSG B, several other solutions significantly exceed or closely approach the lower threshold set by by FreeGrid ($\widehat{LF}$ = 1) for both load conditions (A, D2.1, D2.2, D2.3, D3.4, D3.5);

-in terms of displacements, none of the proposed solutions meet the upper threshold set by FreeGrid (δ = 1/200 = 0.15) when employing the same cross-section for the grid members. Notably, large displacements comparable to those of the DBG occur in LC_2 for DSGs A, C, D1.5, D2.1, where the geometric non-linearity effects are significant.

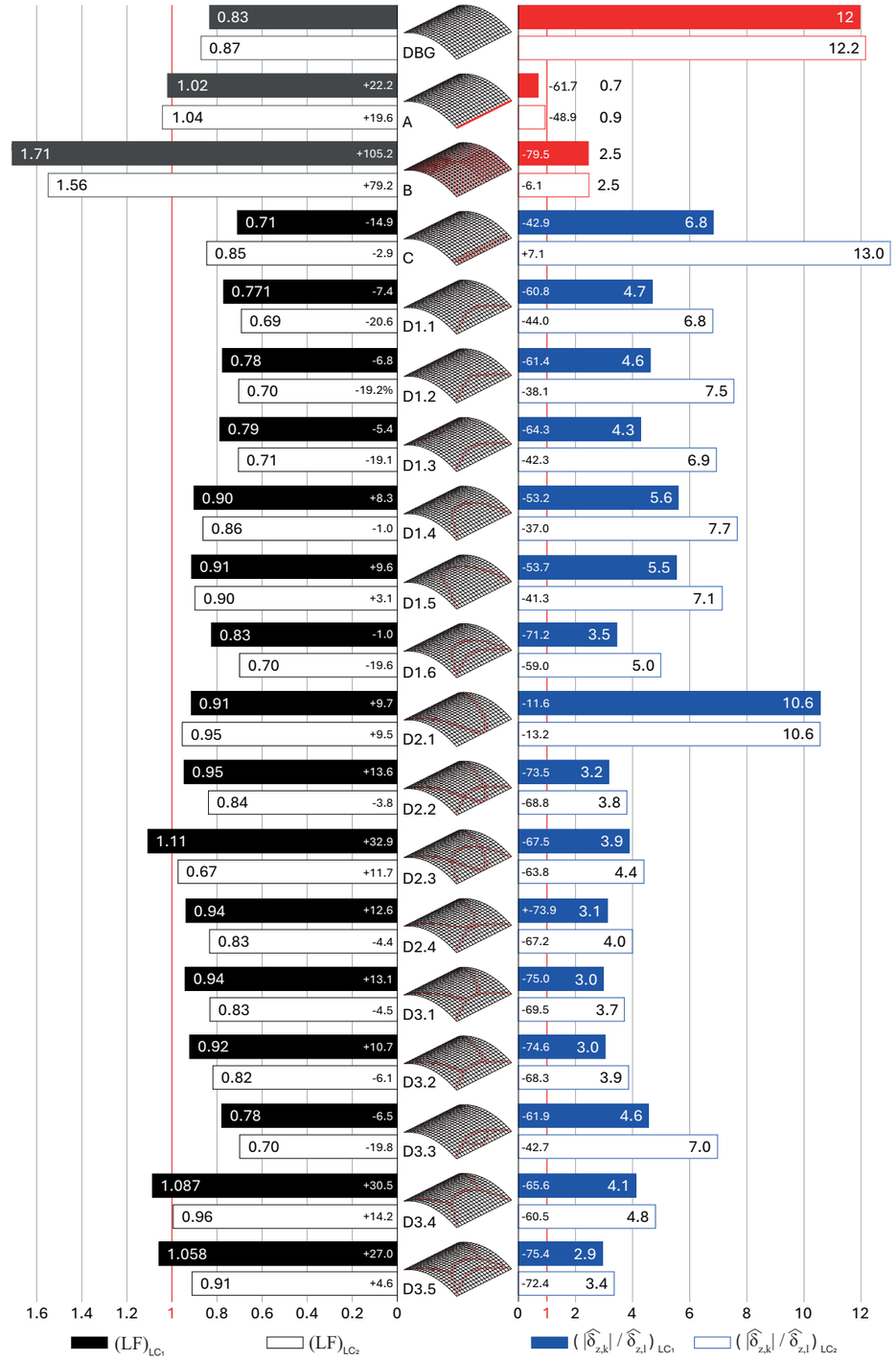

Figure 4.9: Critical Load Factors and maximum displacement values in LC_1 and LC_2

To better understand the comparison between all the proposed DBGs, the structural partial metric P_s was calculated for each solution. In Figure 4.10, the partial metrics are grouped by type, allowing for a simultaneous comparison of the critical Load Factor and the ultimate displacement for each DSGs and DBG.

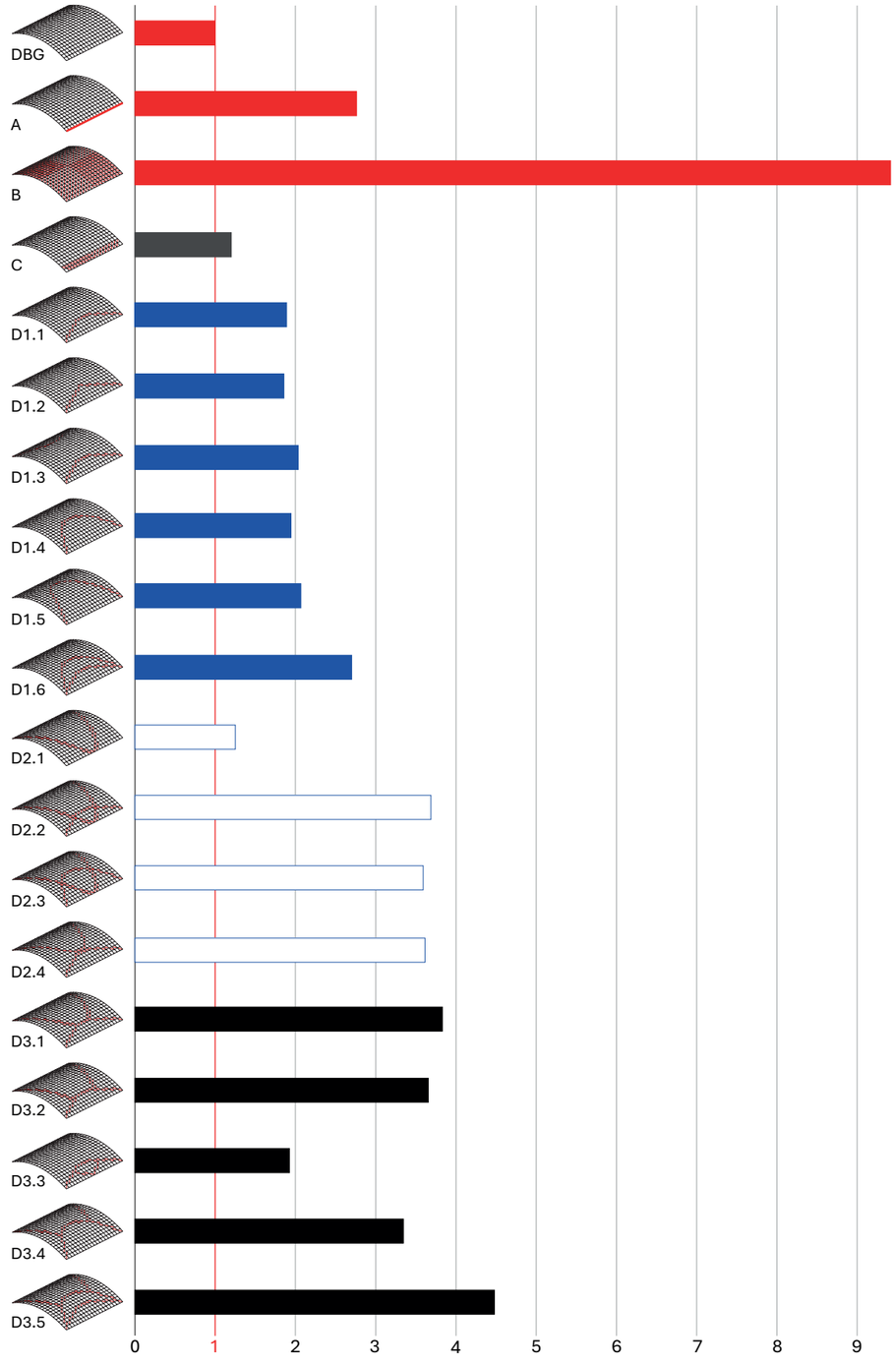

Figure 4.10: Structural performance metrics for DSGs and DBG

Chapter

5

Structural analysis and performance assessment

The in-depth structural analysis focuses on a limited selection of DSGs from Section 4.2, chosen among the three reference solutions and those with the highest Structural performance. Each DSG is analyzed under the asymmetric load condition LC_2, identified in Section 4.3 as more demanding than the symmetric one LC_1.

The detailed analysis of the DBG presented in Section 3.7.2, is included to enable comparison of each DSG behaviour with respect to the baseline geometry;

-DSGs A and B serve as references as they align with practice traditional design solutions -achieved through free-edge stiffening and triangulation of cells, respectively;

-DSG D1.4 (relieving arch with $r = L/2$) is selected as the relieving arch with rise equal to $L/2$ represents the effective limit among relieving arch solutions with variable rise, as demonstrated in Section 4.3. It also shows the highest Structural performance in this latter category;

-no case is selected from category D2 (relieving arch and flying buttress-like) as members discretizing the flying buttress-like prove inactive below the rise of the intersecting relieving arch, as shown in Section 4.3;

-DGSs D3.4 and D3.5 are selected from D3 category (relieving arch and flying buttresses). Specifically, D3.4 (relieving arch with $r = L/2$ and flying buttresses) is chosen to evaluate the effect of adding flying buttresses to DSG D1.4. In addition to this, it is the only DSG in D3 category to approach the lower critical Load Factor threshold $LF_1 = 1$. D3.5 (relieving arches with r=L/2, r=L/4 and flying buttresses) is selected for its highest Structural performance across all DSGs in D1, D2, D3 categories. This configuration combines highest-performing solutions in D1 (D1.6, relieving arches with $r = L/2$, $r = L/4$) and D3 (D3.4) In this way, it thus allows the assessment of the flying buttresses contribution to DSG D1.6.

ULS and SLS analyses **5.1.0**

The ULS analysis is taken under load condition LC_2 and provides the load-displacement curves of the aforementioned solutions (Figure 5.1-a, b, c, d, e, f). In general, the selected solutions in D1 and D3 categories reach ULS due to global

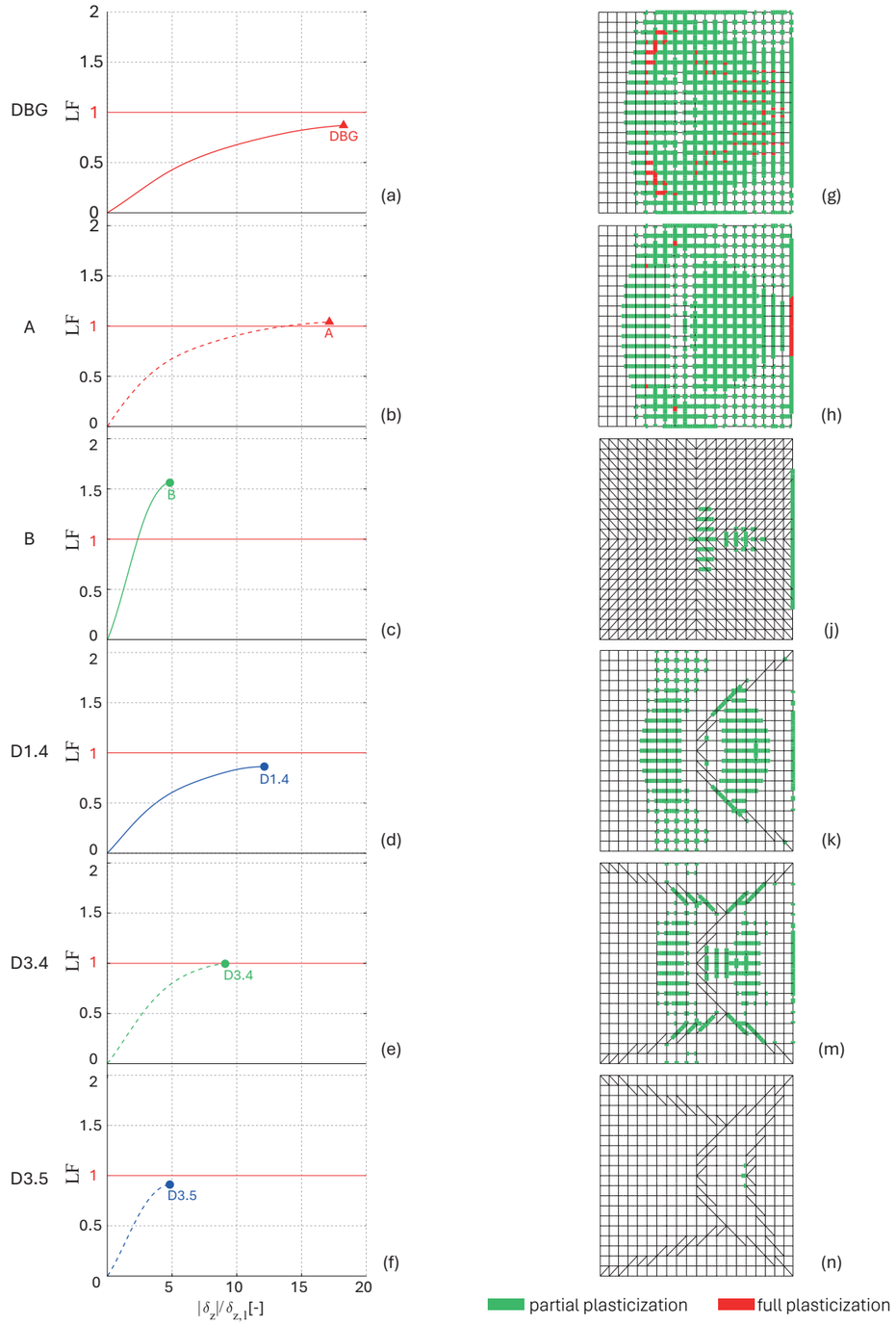

Figure 5.1: Load-displacement curves and yielded FE in LC_2

instability and in quasi-elastic regime in D3.5 (Figure 5.1-f). By contrast, the reference DSG A keeps achieving ULS through full plasticization of members (Figure 5.1-b) similarly to the DBG, while B reaches ULS due to global instability (Figure 5.1-c). Specifically, DSGs D1.4, D3.4, D3.5 show a progressive increase in stiffness compared to the DBG and DSG A, a gradual decrease of partially plasticized members and the absence of fully plasticized ones (Figure 5.1-k, m, n), which still occur in DSG A (Figure 5.1-h). This progressive reduction supports reaching ULS through global instability and quasi-elastic regime for D3.5 -where the number of partially plasticized members is significantly decreased (Figure 5.1-n)-, further confirming the dominance of membrane behaviour over bending behaviour.

The SLS analysis assessed the nodal displacements -both normal and tangential-, axial normal forces and bending moments for the selected DSGs. Each solution is compared to the corresponding evaluations obtained from the DBG analysis.

Figure 5.2 shows the normal $\delta_{\perp}$ (Figure 5.2-a, b, c, d, e, f) and tangential $\delta_{//}$ (Figure 5.2-g, h, j, k, m, n) displacements of DSGs, normalized with respect to the corresponding maximum displacement values among the solutions -as well as those of the DBG ($\delta_{\perp max}$=1.82 m, $\delta_{//max}$=0.44 m).

In general, the results show a progressive decrease in both normal and tangential displacements, starting with the insertion of the relieving arch with a rise $r = L/2$ (D1.4) (Figure 5.2-d, k), followed by the addition of the flying buttresses (D3.4) (Figure 5.2-e, m), until the placement of a second relieving arch with a rise $r = L/4$ (D3.5) (Figure 5.3-f, n). As demonstrated by the ULS analysis in load-displacement curves (Figure 5.1-a, b, c, d, e, f), stiffness progressively increases with the increase of triangular cells. This latter strategy results in decreasing in-plane deformability and, consequently, both normal and tangential displacements. Proof of this is given by the behaviour of DSG B, where the triangulation of all cells results in the lowest displacements among the selected DSGs (Figure 5.2-c, j). Similarly, the observed progressive reduction in displacements among DSGs D1.4, D3.4, D3.5 aligns with the increasing number of triangular cells.

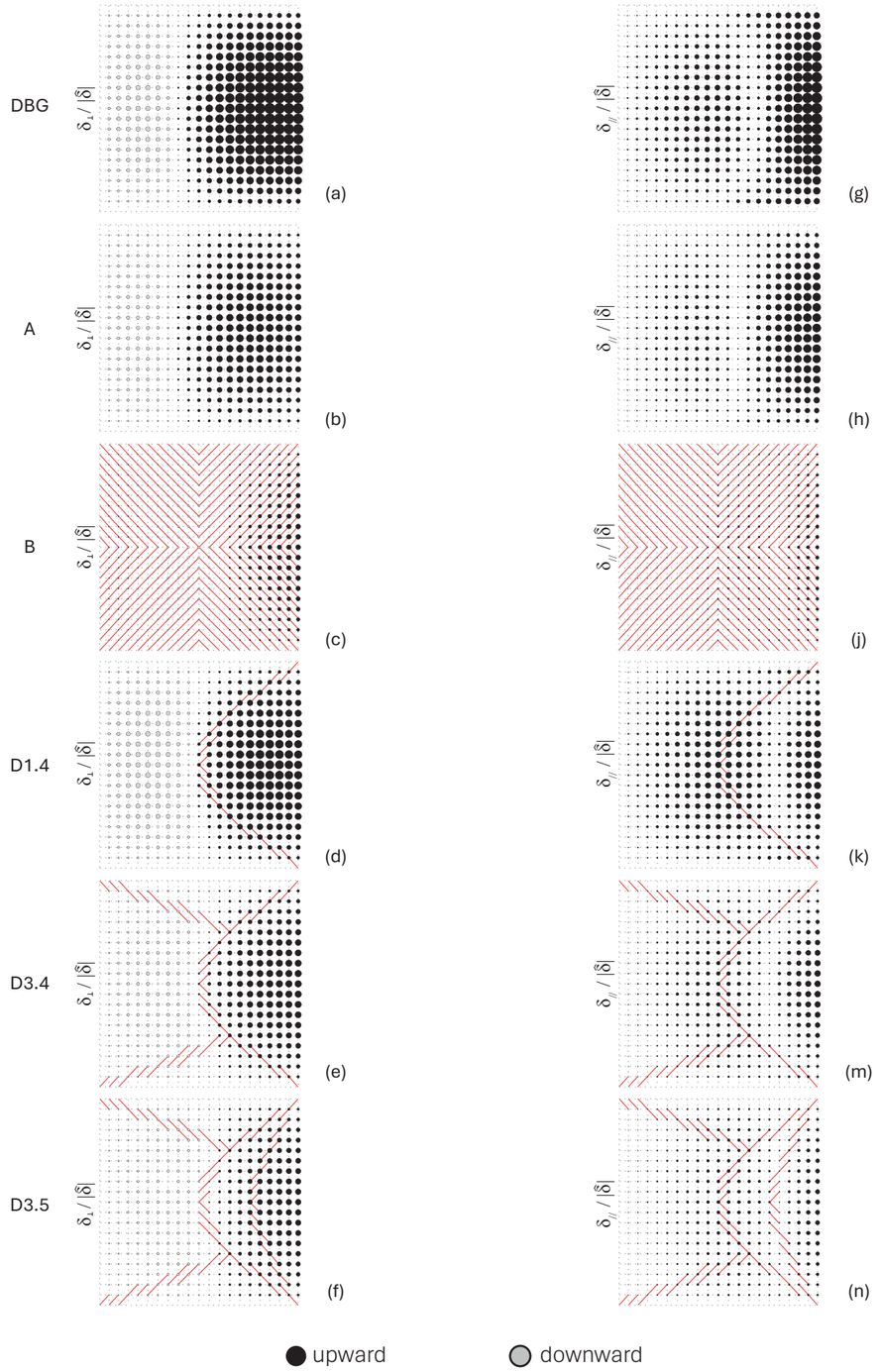

Figure 5.2: Normal and tangential displacements in LC_2

Specifically:
-DSG D1.4 achieves a reduction in normal (Figure 5.2-d) and tangential (Figure 5.2-k) displacements compared to the DBG, but uniquely in the area between the maximum rise and the free edge. As a matter of fact, the magnitude of both displacements remains nearly unchanged in the area between the maximum rise and the constrained edge;
-the addition of the flying buttresses in DSG 3.4 further contributes to decrease both normal and tangential displacements, even affecting the region above the relieving arch (Figure 5.2-e, m);
-the placement of a second relieving arch in DSG D3.5 results in an even greater reduction of normal and tangential displacements. It is noteworthy that these latter are comparable to the displacements observed in DBG, when considering the area beneath the relieving arch and the higher rise. Thus, the strategy employed in this solution proves effective in decreasing normal and tangential displacements to a level almost equivalent to the DSG B, by employing a significantly smaller number of additional members. In terms of maximum displacements, the combination of a pair of relieving arches and flying buttresses performs similarly to the triangulation of each cell.
The stiffening of the free-edge in DSG A results in a reduction of approximately half the DBG normal displacements, while the tangential ones to a lesser extent. The displacements pattern maintains the same distribution as in DBG, except for members nearby the free-edge. The increased stiffness of members along the free-edge enables a reduction in normal displacements along the *x*-axis.
Additionally, a relevant aspect emerging from the comparison between DSGs and DBG considers the displacement pattern. It is observed that all solutions retain a displacements distribution similar to the DBG one.

Figure 5.3 Shows the deformed shapes of the arches for each selected DSG and the deformed and undeformed curve of the DBG. All the solutions reduce vertical displacements with respect to the DBG, with DSG B showing the most efficient as its curve closely aligns with the undeformed shape, for $B<L/4$. DSGs D3.4 and D3.5 also prove effective in reducing downward displacements due to the flying buttresses.

They approximate the undeformed arch within $B<L/2$, i.e in correspondence of the rise of the relieving arch equal to $r=L/2$. The addition of a second relieving arch with rise $r=L/4$ in DSG D3.5 further enhances its effectiveness. Similarly to D3.4, DSG D1.4 proves effective in reducing downward displacements of the DBG within $B<L/2$. However, in the domain $L/4<B< L$, DSG D1.4 is less effective that DSG A, which approximates the deformed shapes of the arches of D3.4 and D3.5 within the same range, due to the stiffening of the members along the free-edge.

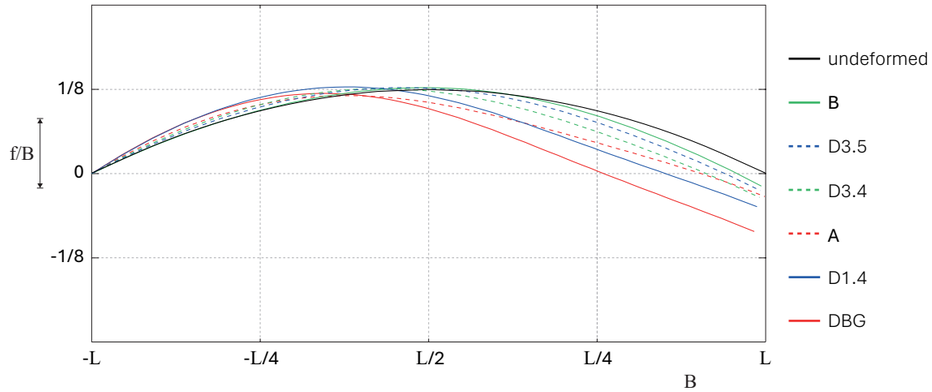

Figure 5.3: Deformed shapes of the DSGs arches at SLS in LC_2

Figure 5.4 presents the SLS analysis of normalized normal forces $N^* = N / |\widehat{N}|$ (Figure 5.4-a, b, c, d, e, f) and bending moments $M^* = M / |\widehat{N}|b$ (Figure 5.4-g, h, j, k, m, n), where $|\widehat{N}|$ is the maximum normal force of the DBG and b is the characteristic length of structural members. This normalization enables the comparison of both magnitude of axial forces and bending moments, as well as the assessment of the predominant membrane or bending behaviour in each DSGs.

In light of the latter aspect, an initial consideration arises from comparing DSGs D1.4, D3.4, D3.5. The analysis of their normal force distributions (Figure 5.4-d, e, f) alongside their bending moment distribution (Figure 5.4-k, m, n) shows that membrane behaviour prevails over the bending one. Consequently, these configurations progressively restore the characteristic mechanical behaviour of gridshells, as opposed to the bending behaviour of the DBG. Specifically:

-DSG D1.4 still exhibits a significant bending behaviour (Figure 5.4-k), although reduced compared to the DBG. The clear contribution of added relieving arch displays in the behaviour of members along the free-edge, where membrane regime predominantly prevails. Greater compressive normal forces $N^*>0$ occur in members forming the relieving arch, while tensile forces $N^*<0$ are concentrated in members along the free-edge. These latter thus act as a chain, countering the thrust of the relieving arch (Figure 5.4-d);

-DSG D3.4 maintains behaviour similar to that of the single relieving arch solution. Unlike this latter, the integration of flying buttresses further increases the predominance of membrane behaviour (Figure 5.4-e) over bending behaviour (Figure 5.4-m);

-the same considerations can be extended to DSG D3.5, where the addition of the second relieving arch lets the prevalence of membrane behaviour to be even more evident (Figure 5.4-f).

The triangulation of cells in DSG B also re-establishes a predominantly membrane behaviour (Figure 5.4-c). By contrast, in reference solution A still occurs flexural behaviour, with stress level comparable to those of the DBG in members along the x-axis. Furthermore, the increase in cross-section of members along the free-edge concentrates bending moments at the boundary (Figure 5.4-h), while reducing the magnitudes in

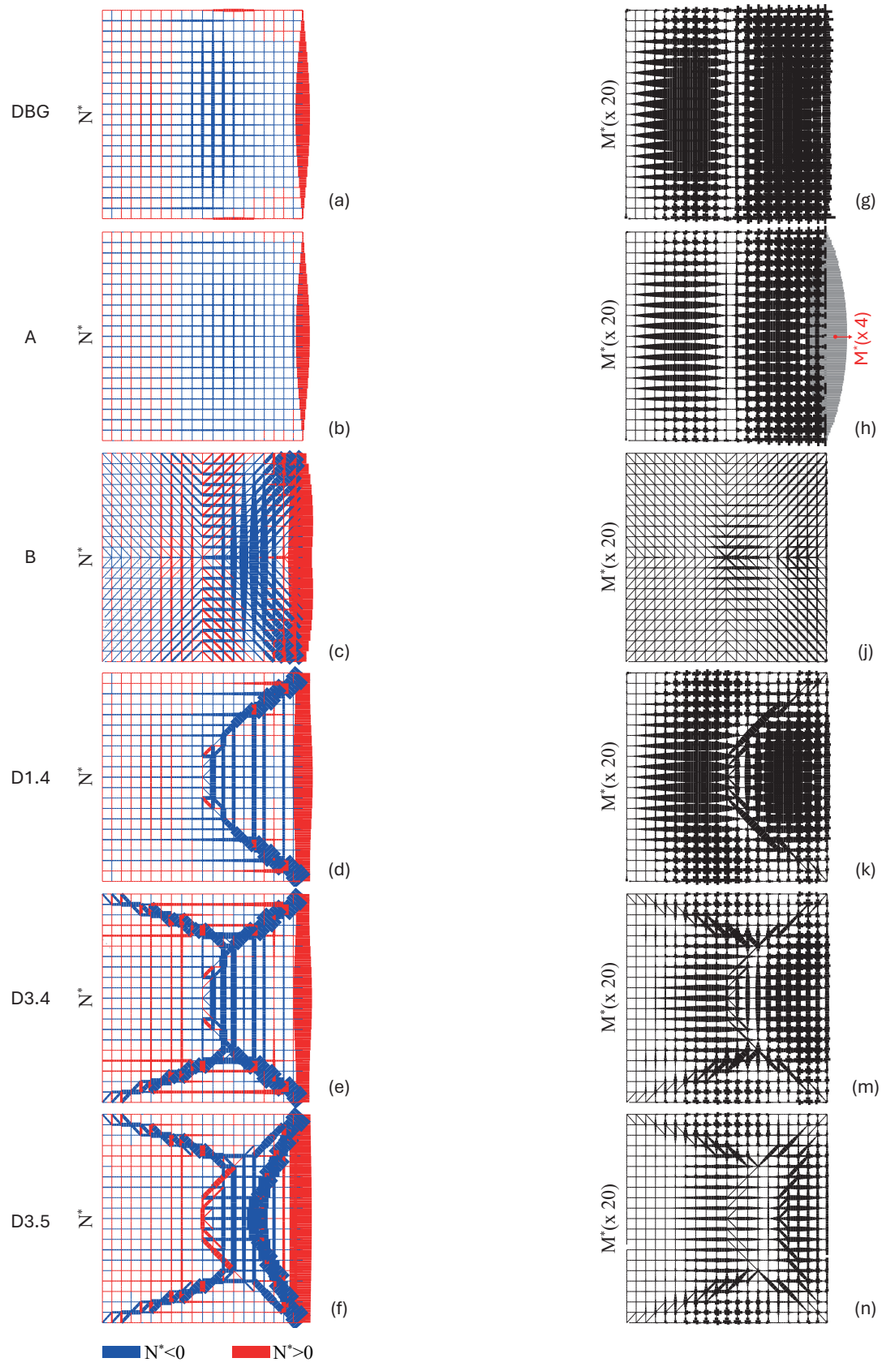

Figure 5.4: Distribution of normalized axial forces and resulting bending moments in LC_2

members along the *y*-axis.

A further consideration can be drawn by examining the axial force distributions across the solutions (Figure 5.4- a, b, c, d, e, f). In all cases, members along the free-edge are subjected to tensile stress, with progressively increasing magnitudes in DSGs D1.4, D3.4, D3.5. The stress distribution in DSG B exhibits a pattern similar to that of a compression-bearing arch (Figure 5.4-c), as indeed confirmed in solutions where a relieving arch is actually placed.

DSGs D1.4, D3.4, D3.5 exhibit a concentration of axial forces in the added members. Compressive stresses are concentrated in the diagonals discretizing the relieving arch with rise $r=L/2$ and in the flying buttresses, for solutions D1.4 and D3.4. Similarly, the flying buttresses are predominantly under compression in D3.5, while members of the relieving arch with rise $r=L/2$ show tensile stresses until they intersect with the flying buttresses. The second relieving arch is primarily subjected to compressive axial forces, behaving similarly to the relieving arch with a rise $r=L/2$ in D1.4 and D3.4.

The magnitude of compressed members along *y*-axis increases as the relieving arch approaches its maximum rise. Members located between the constrained edge and the maximum rise predominantly exhibit compression along *x*-axis and tension along *y*-axis. In DSGs D3.4 and D3.5 tensioned members take place also along *x*-axis nearby the flying buttresses.

The analyses presented in Figure 5.4 are summarized in Figure 5.5 in terms of average values (Figure 5.5-a) and coefficient of variation (Figure 5.5-b) among the members.

Figure 5.5-a underscores the dominance of either membrane or bending behaviour among DSGs, with DSG B standing out as the solution exhibiting the most significant predominance of membrane behaviour.

On the other hand, Figure 5.5-b highlights the increase in the maximum bending moment modulus in DSG A, which shows the highest relative standard deviation compared to the mean.

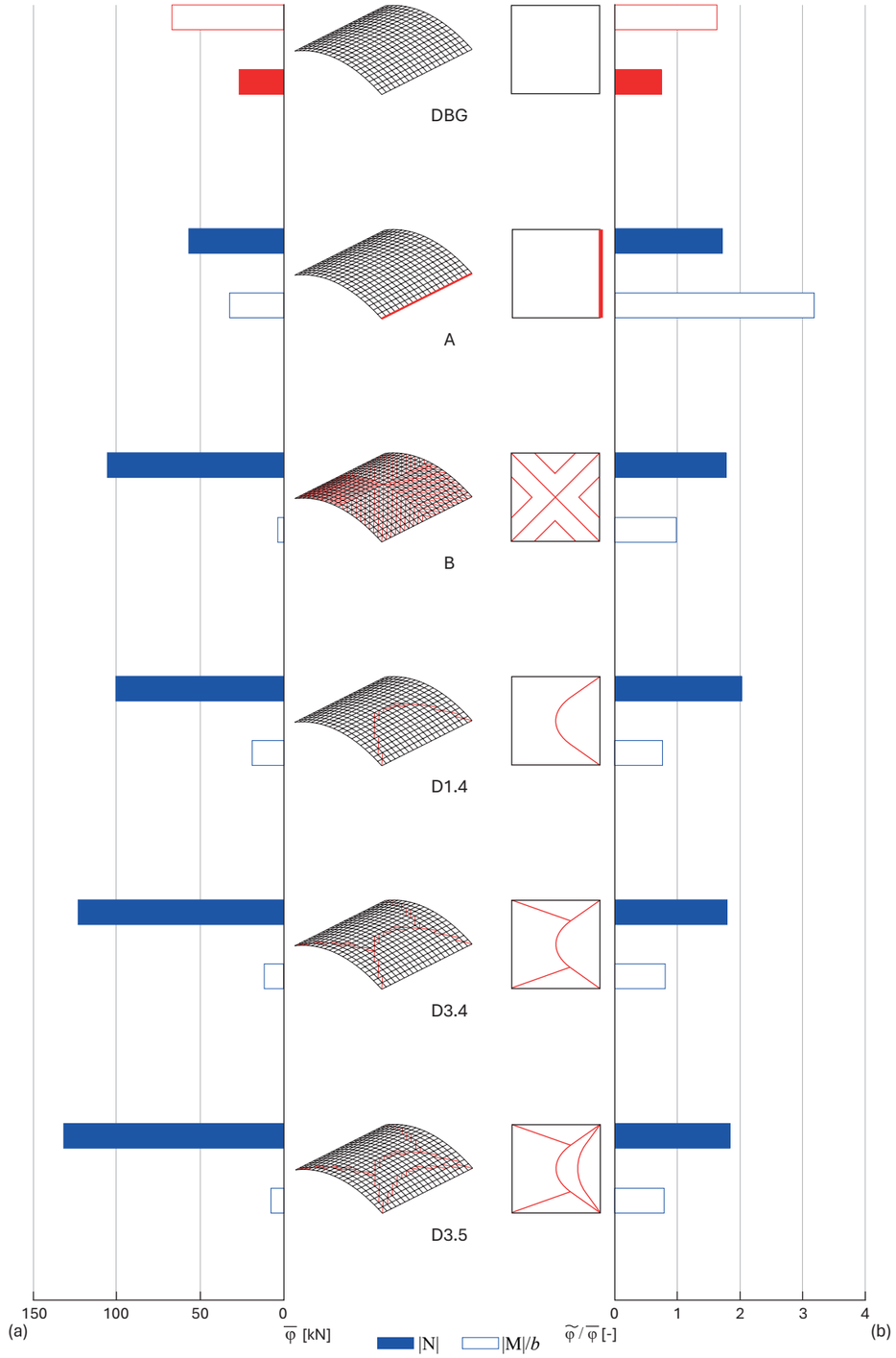

Figure 5.5: Distribution of $|N|$ and $|M|/b$: average value (a) and coefficient of variation (b)

Holistic assessment 5.2.0

Figure 5.6 summarizes partial metrics for Structural performance P_s, Buildability performance P_b, Sustainability performance P_{su} and the overall performance metric P for each selected DSGs. As defined in Section 3.4, each metric reflects an increase or decrease in performance with respect to the DBG, to which they are normalized. Thus, a metric value exceeding the unit value means an improvement in the corresponding performance.

Specifically, DSGs D1.4, D3.4, D3.5 reveal a progressive increase in Structural performance P_s, reaching values up to four times greater than that of the DBG. Similarly, although to a lesser extent, DSG A achieves a comparable outcome, while DSG B achieves twice the Structural performance observed in D3.5.

Buildability performance metric P_b is for all cases lower than the DBG due to the increased variety of joint types and properties of the added members. Specifically:

-DSG A shows a decrease in the P_b metric due to the increased cross-section of members along the free-edge, while maintaining the same joint type across all nodes;

-DSG B exhibits the greatest reduction in P_b driven by the rise in joint types. This latter is required by the higher number of converging members, with up to eight members at the middle joint of the gridshell;

-the same trend as the previous is also observed in DSGs D1.4, D3.4, D3.5.

Sustainability performance P_{su} shows a decrease across the DSGs due to the increased weight of structural material used, as outlined in Section 3.4. This is underscored by the significant decrease in P_{su} for DSG B, where the higher number of added members demands a greater material use and, consequently, a worsening environmental impact coefficient.

Overall, Structural performance emerges as the most significant metric, strongly influencing the global performance P.

Similarly to Structural performance P_s, the Bulk performance values are notably higher for DSGs B and D3.5, despite the reduction in Buildability and Sustainability performances when compared to the other DSGs.

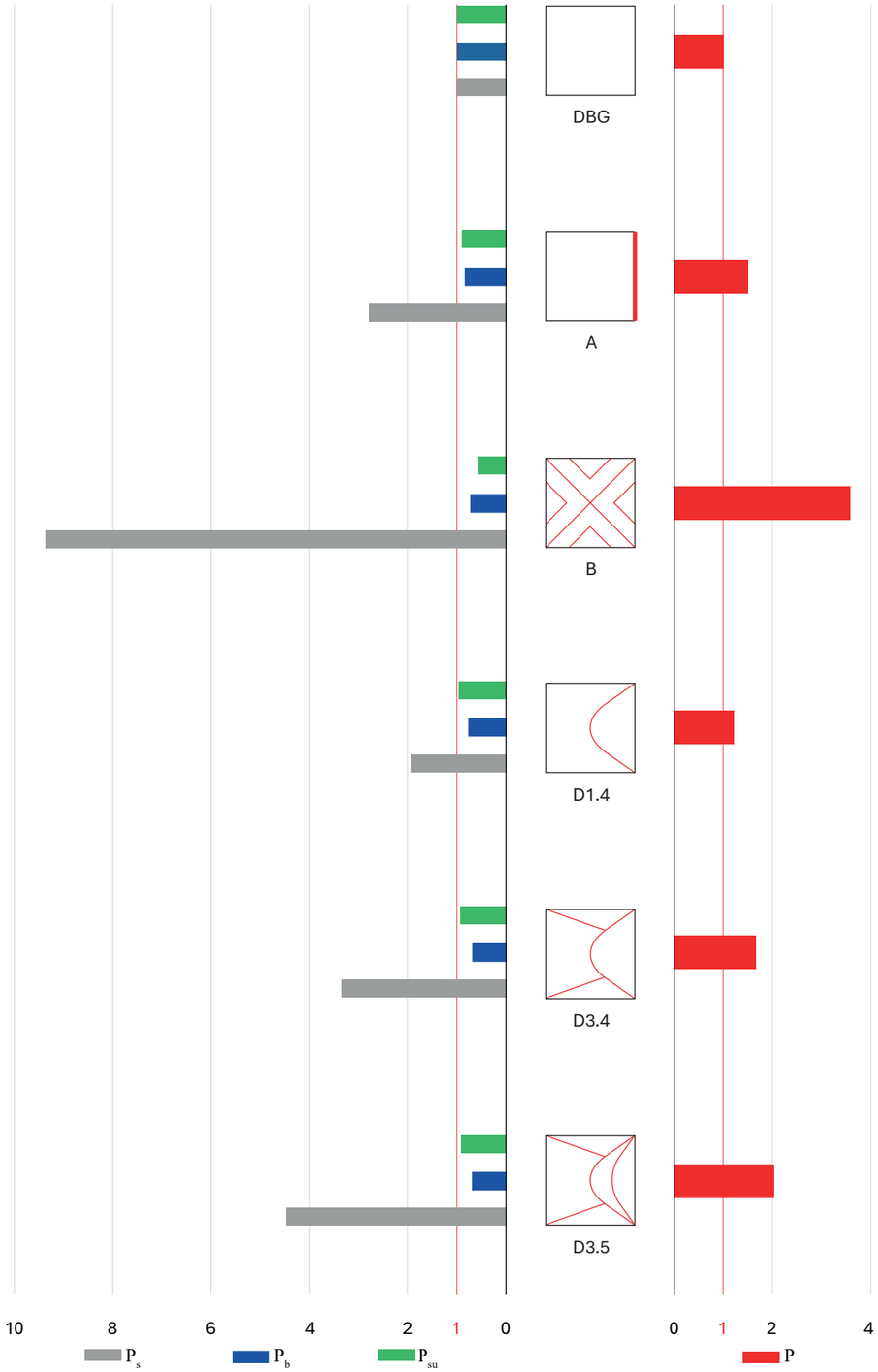

Figure 5.6: Scheme of Partial and Global performance metrics

Chapter

6

Conclusions

Among the strategies employed for the construction of long-span roofs, gridshells derive their efficiency primarily from their geometric configuration. These structures are defined as form-resistant, meaning that they are capable to span large distances due to the shape they assume. This results in a minimal thickness and reduced weight of structural members, which determine their predominantly membrane-like behaviour.

A subset of this category includes free-edge gridshells, obtained by trimming the reference surface in order to be integrated with pre-existing structures or provide access to the building. In light of these advantages, their application has become widespread in the design of large-span buildings such as stadia, hangars and pavilions.

However, the presence of free-edges significantly affects the characteristic behaviour of gridshells, potentially shifting from membrane-like to a flexural regime and leading to large displacements. The widespread application of these structures contrast with the limited scientific research, leaving the stability of free-edge gridshells as a largely unexplored field.

The present MSc Thesis contributes to the research field on free-edge gridshells by proposing design solutions and evaluating their structural performance. The study was conducted with reference to the FreeGrid benchmark, with the aim of bridging the gap between practical design and scientific literature. More precisely, the thesis focuses on the barrel vault gridshell proposed by the benchmark as one of the reference geometries, with the primary objective to enhance its structural performance. The proposed solutions were holistically assessed through the evaluations of Structural, Buildability and Sustainability performances outlined by the benchmark.

Chapter 1 introduced motivations and conditions that led to the definition of gridshells as a structural typology. It highlights how advancements in materials technology and their intrinsic properties have contributed to the efficiency of this structural type, enabling the achievement of goals often unattainable with other structural systems.

Chapter 2 delves into various aspects related to the architecture of gridshells. The discussion includes, on one hand, an analysis of morphology which demonstrated the origin of

the form-resistant structures concept. On the other hand, it classifies gridshells with respect to construction methods, boundary conditions, geometric characteristics and materials that can influence their structural behaviour. This section highlights how buckling instability remains the most significant factor affecting gridshell performance and serves as primary cause of structural failure. Furthermore, it underscores the ongoing lack of research on the free-edge gridshells stability.

Chapter 3 provides an in-depth overview of the FreeGrid benchmark, outlining its objectives, methodologies and technical specifications, which served as the guideline framework for the analyses undertaken in this study. An in-depth analysis of the barrel vault Design Baseline Geometry (DBG) revealed how its single curvature significantly impacts on the mechanical behaviour, leading to high displacements values. Additionally, the assessment demonstrated that:

- the free-edge boundary effects are prevailing over the effects of the load conditions on the DBG structural behaviour;
-the Ultimate Limit State (ULS) is reached in a locally-plastic regime due to the plasticization of one or more structural members;
- the highest axial forces are concentrated in members along the free-edge, which are subjected to tensile force;
-flexural behaviour prevails over membrane behaviour due to the insufficient in-plane stiffness of the vault.

The proposed Design Solution Gridshells (DSGs) are detailed in Chapter 4. DSGs draw inspiration both from strategy commonly used in built free-edge gridshells (e.g., cells triangulation, stiffening of the free-edge) as well as from unconventional approaches (e.g., truss-girder, relieving arches). Preliminary analyses of each DSGs are discussed according to the employed category of strategy. The findings proved that:

-the complete triangulation of the grid cells and fully quad mesh pattern define the range within which all other solutions fall;
-the stiffening of the free-edge by using a larger cross-section does not provide sufficient stiffness. Notably, this latter goal is not achievable even with the larger commercially available cross-section, in addition to a significant impact on the architectural outcome;

-adding a truss-girder to stiffening the free-edge does not effectively reduce out-of-plane displacements, as it lies on the reference surface and thus uniquely effective within in-plane displacements;
-the addition of a relieving arch proves effective, especially when the rise is at most half the span of the gridshell;
-the combination of flying buttresses with relieving arches proves to be the most effective strategy in terms of Structural performance, as it limits out-of-place deformations of the relieving arches and restores the characteristic membrane-like behaviour.

Chapter 5 dealt with the detailed Ultimate Limit State and Serviceability Limit State analyses of a selected number of DSGs, chosen from those previously assessed and identified as the most efficient in Structural performance across all categories. The analyses stated the following findings:
-all the selected DSGs successfully restore the membrane-like behaviour and, as a result, remove the presence of fully plasticized members;
-increasing the number of triangulated cells reduces displacements, the number of partially plasticized members and the magnitude of bending moments;
-Structural performance, as well as Bulk performance, improves for all the selected DSGs, albeit with a minimal worsening in terms of Buildability and Sustainability performances;
-some solutions manage to meet or approach the lower critical Load Factor threshold set by the benchmark, while none satisfy the upper limit for maximum displacement.

In light of these considerations, the present MSc Thesis has contributed to the definition of design solutions for free-edge gridshells, specifically through the barrel vault geometry proposed as a reference by the FreeGrid benchmark.
The main contributions can be summarized as follows:
-the identification of limits and peculiarities of each tested strategies;
-the evaluation of the effects of both traditional solutions from the design practice of free-edge gridshells and unconventional ones, through the assessment of the mechanical behaviour in terms of critical Load Factor and maximum displacements;
-the formulation of a design response aimed at restoring the membrane-like behaviour, which is compromised by free-edges;
-a holistic assessment of the solutions in terms of Structural, Buildability and Sustainability performances.

Future directions opened up by the present study aim to meet both ULS and SLS requirements set by FreeGrid, which have so far been achieved or approached uniquely in terms of Load Factor, while the upper displacement limit remains a fully unmet goal. The strategies suggested by this study for further tests concern:
-the appropriate sizing of the structural members added to the reference grid, potentially through an optimization process;
-the variation of the reference geometry shape according to the limits set by the benchmark. In this regard, a few scenarios have already been experimented, revealing themselves as potentially efficient solutions. These latter involved geometric variation of the free-edge in a parabolic arch shape, once again following a design from precedent approach, based in this case on the experimental studies of Heinz Isler (Figure 6.1). The v includes a lunette-like surface intersecting the original vault surface (Figure 6.2), designed to contain out-of-plane displacements. This solution proved effective only if the spring nodes of the boundary arch are prevented to move in horizontal direction, e.g., by constraining their y-wise displacements or by inserting a chain to contrast the arch thrust. Both these solutions do not meet some of the benchmark constraints, therefore further studies are needed.

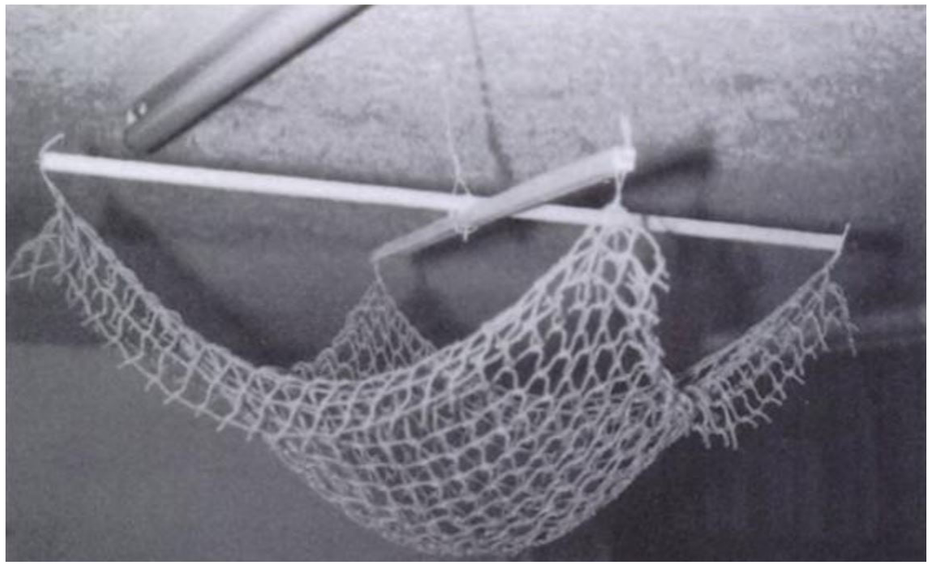

Figure 6.1: Hanging membrane model with upturned stiffened free edges, Heinz Isler (Chilton, 2000)

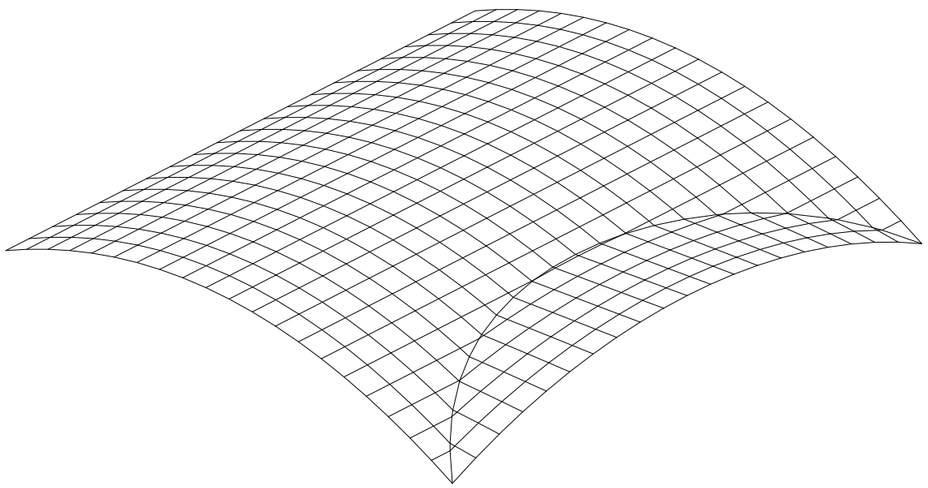

Figure 6.2: Scheme of preliminary evaluated DSG with a lunette-like

Bibliography

Ahmed A. M., Rifai, A.M, *Euler-Bernoulli and Timoshenko Beam Theories, Analytical and Numerical Comprehensive Revision*, European Journal of Engineering and Technology Research, vol. 6, p. 20-32, 2021.
DOI: 10.24018/ej-eng.2021.6.7.2626

Abel J.F, Chilton J. C., *Heinz Isler: Years of "New Shapes for Shells"*, Journal of the International Association for Shell and Spatial Structures: IASS, vol. 52(3), p.131-134, 2011.

Block P. et al, *As Hangs the Flexible Line: Equilibrium of Masonry Arches*, Nexus Network Journal, vol. 8, p. 13-24, 2006.

Boling E., *The Nature and Use of Precedent in Designing in: Design for Learning: Principles, Processes, and Praxis*, BYU Open Learning Network, 1st edition, 2021.

Boller G. *et al*, *Heinz Isler's physical form finding of the HIB tennis shells*, Structures, vol. 65,2024.
DOI:10.1016/j.istruc.2024.106559

Bordigoni Pistorello S. *et al*, *FreeGrid Benchmark: soluzioni progettuali per una volta a botte reticolare in acciaio con imposta parzialmente vincolata*, XXIX Congresso C.T.A, Milano, 2024.

Bruno L., Venuti F., *Influence of in-plane and out-of-plane stiffness on the stability of free-edge gridshells: A parametric analysis*, Thin-Walled Structures, vol.131, p.755–768, 2018.
DOI: 10.1016/j.tws.2018.07.019

Bruno L. *et al*, *Freegrid: a benchmark on design and optimisation of free-edge gridshells*, Proceedings of the IASS Annual Symposium 2023, Melbourne, 2023-a.

Bruno L. *et al*, *Exploring new frontiers in gridshell design: The FreeGrid benchmark*, Structures, vol.58, 2023-b.
DOI: 10.1016/j.istruc.2023.105678

Bruno L. *et al*, *FreeGrid overview*, FreeGrid Benchmark, Tech. Rep, 2023-c.
[Online] Available https://sites.google.com/view/freegrid

Bruno L. *et al*, Ts01: *Baseline setup*, FreeGrid Benchmark, Tech. Rep, 2023-d.
[Online] Available https://sites.google.com/view/freegrid.

Bruno L. *et al*, Ts02: *Design constraints*, FreeGrid Benchmark, Tech. Rep, 2023-e.
[Online] Available https://sites.google.com/view/freegrid.

Bruno L. *et al*, Ts03: *Finite Element model*, FreeGrid Benchmark, Tech. Rep, 2023-f.
[Online] Available https://sites.google.com/view/freegrid.

Bruno L. *et al*, Ts04: *Performance metrics*, FreeGrid Benchmark, Tech. Rep, 2023-g.
[Online] Available https://sites.google.com/view/freegrid.

Bruno L. *et al*, *Design Solutions for the barrel vault FreeGrid Design Baseline Gridshells*, Proceedings of the IASS Annual Symposium 2024, Zurich, 2024-h.

Bulenda T., Knippers J., *Stability of grid shells*, Computers and Structures, vol. 79, p. 1161-1174 2001.
DOI:10.1016/S0045-7949(01)00011-6

Carlini A., Tedeschini Lalli L., *A Metallic 1928 Geodesic Dome in Rome*, Proceeding of the 18th Conference on Applied Mathematics, 2019.

Chilton J.C., *Timber Gridshells, Architecture, Structure and Craft*, Routledge, 2016.

Chilton J.C., *Heinz Isler: The Engineer's Contribution to Contemporary Architecture*, ThomaTelford Ltd, 2000.
DOI:10.1680/eccahi.28784

Douthe C. *et al*, *Form-finding of a gridshell in composite materials*, Journal of the International Association for Shell and Spatial Structures: IASS, 47(150), 2006.

Drew P., *Frei Otto, Form and Structures*, Westview Press, 1976.

Dyvik S. H., Mork J. H., *Gridshell Manual*, MSc Thesis, NTNU, 2015.

Dyvik S. H. *et al*, *Gridshell in recent research – a systematic mapping study*, Applied Sciences, vol. 11, 11731, 2021.
DOI:10.3390/app112411731

Faber C., *Candela, the Shell Builder*, Reinhold Publishing Corporation, 1963.

Fan F. *et al*, *A new classification system for the joints used in lattice shells*, Thin-Walled Structures, vol. 49, p. 1544-1553, 2011.
DOI: 10.1016/j.tws.2011.08.002

Fernandes J. *et al*, *Tectonic Design of Elastic Timber Gridshells*, World Conference on Timber Engineering 2016, Vienna, 2016.
Froli M., Laccone F., *Experimental static and dynamics tests on a large-scale free-form Voronoi grid shell mock-up in comparison with finite-element method results*, International Journal of Advanced Structural Engineering, vol. 9, p. 293-308, 2017.

Gioncu V., *Instability problems in space structures*, International Journal of Space Structures, vol. 1(3), p. 169-183, 1985.

Gioncu V., *Buckling of Reticulated Shells – State – of – the -Art*, International Journal of Space Structures, vol. 10(1), p. 1-46, 1995.

Grande E. *et al*, *Role of global buckling in the optimization process of grid shells: Design strategies*, Engineering Structures, vol. 156, p. 260-270, 2018.
DOI: 10.1016/j.engstruct.2017.11.049

IASS WG8 for Metal Spatial Structures, (Draft) *Guide to buckling load evaluation of metal reticulated roof structures*, International Association for Shell and Spatial Structures, 2014.

Kato S. *et al*, *Collapse of semi-rigidly jointed reticulated domes with initial geometry imperfections*, Journal of Constructional Steel Research, vol. 48, p. 145-168, 1998.
DOI: 10.1016/S0143-974X(98)00199-0

Leslie T., *"Laborious and Difficult:" The Evolution of Pier Luigi Nervi's Hangar Roofs*, 1935-1941, 6th International Congress on Construction History (6ICCH 2018), Brussels, 2018.
DOI: 10.13140/RG.2.2.31482.39367

Liddell I., *Frei Otto and the development of gridshells*, Case Studies in Structural Engineering, vol. 4, p.39-49, 2015.
DOI: 10.1016/j.csse.2015.08.001

Liuti A. *et al*, *Where design meets construction: a review of bending active structures*, Proceedings of the IASS Symposium 2018, Boston, 2018.

Majowiecki M., *Structural Architecture for large roofs: concepts and realisations*, Conference "Wettkampf der Arenen", Dusseldorf, 2005.
DOI:10.1002/bate.200590056

Majowiecki M., *Grandi Coperture*, in Almanacco dell'Architetto di R. Piano e C. Piano, Proctor Edizioni, p. 486-589, 2012.

Malek S. R., *The Effect of Geometry and Topology on the Mechanics of Grid Shells*, PhD Thesis, MIT, 2012.

Mesnil R., *Stability of Elastic Grid Shells*, MSc Thesis, MIT, 2013.

Nurdiah E. *et al*, *Bamboo Gridshell: from the material to the structure*, Proceedings of the World World Conference on Timber Engineering, Oslo, 2023.

Pedersen O. E., *The Tectonic Potentials of Concrete*, PhD Thesis, Aarhus School of Architecture, 2013.

Persson R., *Design framework for optimized gridshell structures and their potential applications*, MSc Thesis, Chalmers University of Technology, 2023.

Raffaele L. *et al*, *Holistic performance assessment of gridshells: Methodological framework and applications to steel gridshells*, Journal of Building Engineering, vol. 90, 109406, 2024.
DOI: 10.1016/j.jobe.2024.109406

Rivoli R., *Progettazione strutturale parametrica di strutture a volta: il caso studio della moschea di Dakar*, MSc Thesis, Politecnico di Torino, 2023.

Rockwood D., *Bamboo Gridshells*, Routledge, 2015.

Rossino M., *Concezione e ottimizzazione delle strutture a guscio in muratura*, MSc Thesis, Politecnico di Torino, 2018.

Schlaich J., Schober H., *Glass roof for the Hippo House at the Berlin Zoo*, Strucrual Engineering International, vol. 7, p. 252-254, 1997.

Schlaich M., *Conceptual design of light-weight structures*, lsaa, 2011.

Schober H., Justiz S., *Cabot Circus, Bristol Ebene Viereckknetze für freigeformte Glasdächer*, Stahlbau, vol. 81, p. 28-42, 2012.
DOI:10.1002/stab.201290072

Songel J. M., *Sustainability Lessons from Vernacular Architecture in Frei Otto's Work*, The International Archives of the Photogrammetry, Remote Sensing and Spatial Information Sciences, vol. XLIV-M-1, 2020.
DOI: 10.5194/isprs-archives-XLIV-M-1-2020-233-2020

Tonelli D. *et al*, *Stability of Statics Aware Voronoi Grid-Shells*, Engineering Structures, vol.116, p. 70-82, 2016.
DOI: 10.1016/j.engstruct.2016.02.049

Van der Linden L.P.L., *Innovative joints for Gridshells*, MSc Thesis, TU Delft, 2015.

Venuti F., *Influence of pattern anisotropy on the structural behaviour of free-edge single-layer Gridshells*, Curved and Layered Structures, vol. 8, p. 119-129, 2021.
DOI: 10.1515/cls-2021-0011

Zhang Z. et al, Robustness study of fabricated single-layer gridshell Structures based on sensitivity and vulnerability, Thin-Walled Structures, vol. 180, 109753, 2022.
DOI:10.1016/j.tws.2022.109753